IN THIS JOURNAL

Great Britain Journals Press

journalspress.com

London Journal of Engineering Research

Volume 24 | Issue 5 | Compilation 1.0

Print ISSN: 2631-8474
Online ISSN: 2631-8482
DOI: 10.17472/LJER

COMPILED IN UNITED KINGDOM

ENGLISH

London Journal of Engineering Research

Volume 24 | Issue 5 | Compilation 1.0

PUBLISHER

Great Britain Journals Press
1210th, Waterside Dr, Opposite Arlington Building, Theale, Reading
Phone:+444 0118 965 4033 Pin: RG7-4TY United Kingdom

SUBSCRIPTION

Frequency: Quarterly

Print subscription
$280USD for 1 year
$500USD for 2 year
(*color copies including taxes and international shipping with TSA approved)*
Find more details at https://journalspress.com/journals/subscription

ENVIRONMENT

Great Britain Journals Press is intended about Protecting the environment. This journal is printed using led free environmental friendly ink and acid–free papers that are 100% recyclable.

Great Britain Journals Press Headquaters

1210th, Waterside Dr,
Opposite Arlington
Building, Theale, Reading
Phone:+444 0118 965 4033
Pin: RG7-4TY
United Kingdom

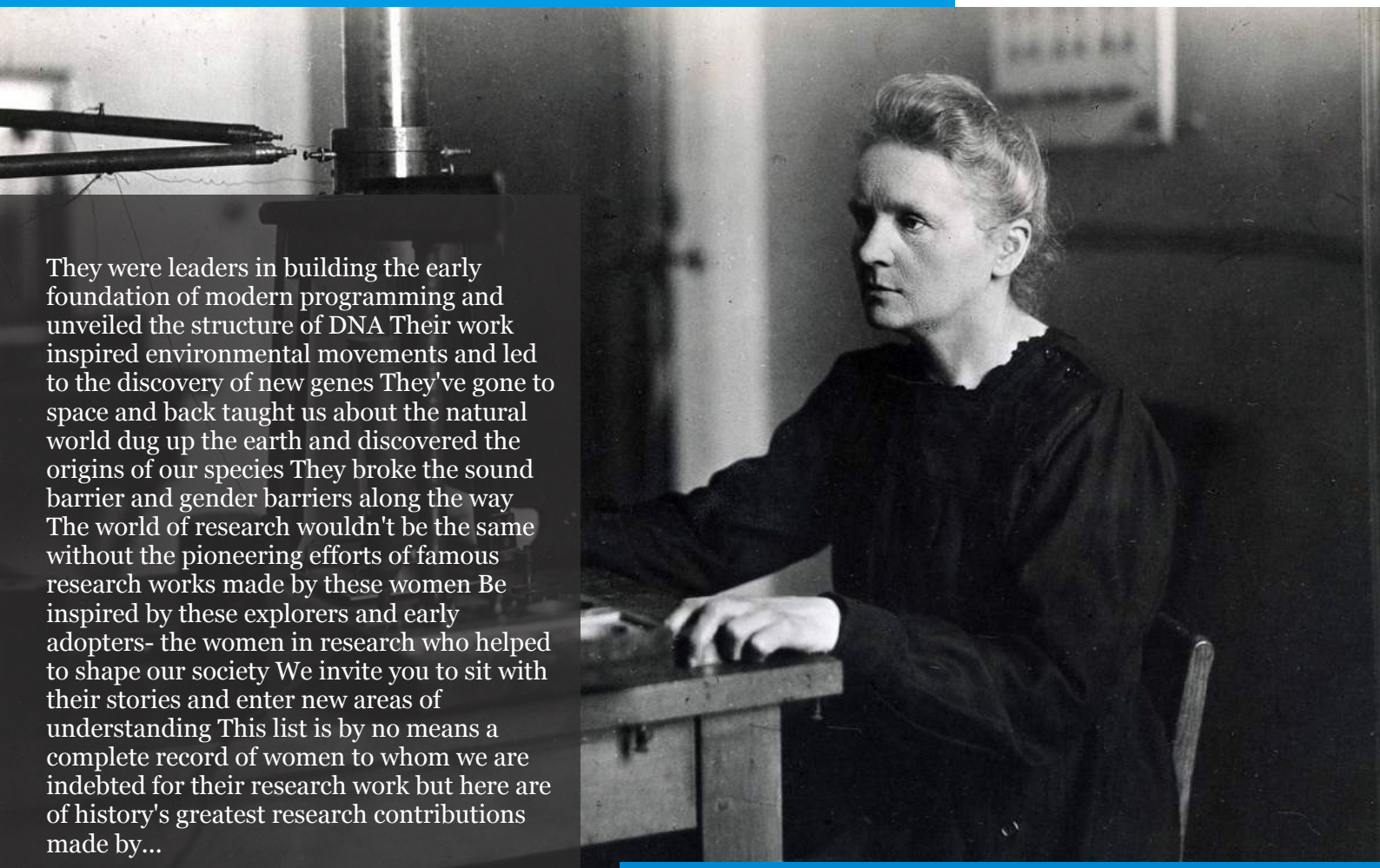

They were leaders in building the early foundation of modern programming and unveiled the structure of DNA Their work inspired environmental movements and led to the discovery of new genes They've gone to space and back taught us about the natural world dug up the earth and discovered the origins of our species They broke the sound barrier and gender barriers along the way The world of research wouldn't be the same without the pioneering efforts of famous research works made by these women Be inspired by these explorers and early adopters- the women in research who helped to shape our society We invite you to sit with their stories and enter new areas of understanding This list is by no means a complete record of women to whom we are indebted for their research work but here are of history's greatest research contributions made by...

Read complete here:
https://goo.gl/1vQ3lS

Women In Research

Computing in the cloud!

Cloud Computing is computing as a Service and not just as a Product Under Cloud Computing...

Read complete here:
https://goo.gl/VvHC72

Writing great research...

Prepare yourself before you start Before you start writing your paper or you start reading other...

Read complete here:
https://goo.gl/np73jP

Journal Content
In this Issue

Great Britain Journals Press

Editorial Board

Curated board members

Dr. Rocío Maceiras

Associate Professor for Integrated Science,
Defense University Center, Spain Ph.D., Chemical
Engineering, University of Vigo, SPAIN

Dr. Rolando Salgado Estrada

Assistant Professor,
Faculty of Engineering, Campus of Veracruz,
Civil Engineering Department, Ph D.,
Degree, University of Minho, Portugal

Dr. Abbas Moustafa

Department of Civil Engineering,
Associate Professor, Minia University, Egypt, Ph.D
Earthquake Engineering and Structural Safety,
Indian Institute of Science

Dr. Wael Salah

Faculty of Engineering,
Multimedia University Jalan Multimedia,
Cyberjaya, Selangor, Malaysia, Ph.D, Electrical and
Electronic Engineering, Power Electronics and Devices,
University Sians Malaysia

Prof. Baoping Cai

Associate Professor,
China University of Petroleum,
Ph.D Mechanical and Electronic Engineering,
China

Dr. Kao-Shing Hwang

Electrical Engineering Dept.,
Nationalsun-Yat-sen University Ph.D.,
Electrical Engineering and Computer Science,
Taiwan

Dr. Mu-Chun Su

Electronics Engineering,
National Chiao Tung University, Taiwan,
Ph.D. Degrees in Electrical Engineering,
University of Maryland, College Park

Nagy I. Elkalashy

Electrical Engineering Department,
Faculty of Engineering,
Minoufiya University, Egypt

Dr. Vitoantonio Bevilacqua

Department of Electrical and Information
Engineering Ph.D., Electrical Engineering
Polytechnic of Bari, Italy

Prof. Qingjun Liu

Professor, Zhejiang University, Ph.D.,
Biomedical Engineering,
Zhejiang University, China

Research papers and articles

Volume 24 | Issue 5 | Compilation 1.0

Decisions with Uncertainty using Deterministic Analysis

José Jesús Acosta Flores

ABSTRACT

The purpose of this article is to present a simple algorithm where an analyst and a decision- maker interact in problems with uncertainty and several objectives.

The algorithm transforms the random problem into a deterministic one by calculating the equivalents under certainty of the alternatives, where the preferences of the decision-maker can be neutrality, constant aversion or constant proneness to risk and the probability functions uniform, normal, exponential, Cauchy, Chi-square, Erlang, Gamma and Laplace.

To solve the deterministic problem, the algorithm applies the modified Proact method to make the interaction with the decision-maker easier. This modification consists of stipulating a value function for two of the measures of effectiveness.

One of the limitations of this algorithm is the existence of a single decider. Another limitation is when the probability functions of the effectiveness measures are not independent.

Keywords: decisions, multiple objectives, random variables, utility functions, value functions, equivalents under certainty, dominance, compensatory swaps.

Classification: DDC Code: 003

Language: English

Great Britain Journals Press

LJP Copyright ID: 392951
Print ISSN: 2631-8474
Online ISSN: 2631-8482

London Journal of Engineering Research

Volume 24 | Issue 5 | Compilation 1.0

Decisions with Uncertainty using Deterministic Analysis

José Jesús Acosta Flores

ABSTRACT

The purpose of this article is to present a simple algorithm where an analyst and a decision- maker interact in problems with uncertainty and several objectives.

The algorithm transforms the random problem into a deterministic one by calculating the equivalents under certainty of the alternatives, where the preferences of the decision-maker can be neutrality, constant aversion or constant proneness to risk and the probability functions uniform, normal, exponential, Cauchy, Chi-square, Erlang, Gamma and Laplace.

To solve the deterministic problem, the algorithm applies the modified Proact method to make the interaction with the decision-maker easier. This modification consists of stipulating a value function for two of the measures of effectiveness.

One of the limitations of this algorithm is the existence of a single decider. Another limitation is when the probability functions of the effectiveness measures are not independent.

Finally, to illustrate the application of the algorithm, a hypothetical example was presented where the best location of an airport is prescribed.

Keywords: decisions, multiple objectives, random variables, utility functions, value functions, equivalents under certainty, dominance, compensatory swaps.

RESUMEN

El propósito de este artículo es presentar un algoritmo simple donde interactúan un analista y un decisor en problemas con incertidumbre y varios objetivos.
El algoritmo transforma el problema aleatorio en uno determinista mediante el cálculo de los equivalentes bajo certeza de las alternativas, donde las preferencias del decisor pueden ser de neutralidad, de aversión constante o de propensión constante al riesgo y las funciones de probabilidad la uniforme, normal, exponencial, Cauchy, Chi-cuadrada, Erlang, Gamma y Laplace.

Para resolver el problema determinista aplica el método ProAct modificado para hacer más simple la interacción con el decisor. Esa modificación consiste en estipular una función valor para dos de las medidas de efectividad.

Una de las limitaciones del presente algoritmo es la existencia de un solo decisor. Otra limitación se tiene cuando las funciones de probabilidad de las medidas de efectividad no son independientes.

Finalmente, para ilustrar la aplicación del algoritmo se expuso un ejemplo hipotético donde se prescribe la mejor localización de un aeropuerto.

Descriptores: decisiones, objetivos múltiples, variables aleatorias, funciones utilidad, funciones valor, equivalentes bajo certeza, dominancia, permutas compensatorias.

Author: Profesor de tiempo completo. División de Ingeniería Mecánica e Industrial. Facultad de Ingeniería. UNAM. Edificio Bernardo Quintana. Piso 3. Facultad de Ingeniería. México D. F.

I. INTRODUCCIÓN

En muchos proyectos se tienen incertidumbre y varios objetivos, por lo que se requiere tener varias medidas de efectividad, al menos una para cada objetivo, y una función utilidad conjunta que evalúe las consecuencias de las decisiones posibles mediante sus medidas de efectividad. Con el fin de tener esa función utilidad hay necesidad de verificar diversos supuestos como la independencia preferencial, la independencia en utilidad y la independencia aditiva, (Keeney and Raiffa, 1976). Dependiendo del cumplimiento de esos supuestos se tienen funciones utilidad de diferentes tipos, que requieren respuestas a preguntas que pueden ser difíciles de contestar para un decisor.

Acosta (2019) desarrolla un algoritmo donde transforma el problema aleatorio en uno determinista y luego aplica el método ProAct para determinar la mejor decisión.

Para transformar el problema aleatorio en uno determinista, Acosta calcula para cada alternativa de decisión i y cada medida de efectividad j, el equivalente bajo certeza, EBC_{ij}, considerando $u(EBC_{ij}) = \int_{-\infty}^{\infty} f_{ij}(x_0)u_j(x_0)dx_0$ donde $f_{ij}(x_0)$ es la función densidad de probabilidad de la medida de efectividad j para la alternativa i; y $u_j(x_0)$ es la utilidad del decisor sobre la medida de efectividad j.

En el primer artículo (Acosta, 2019), se consideran la función densidad de probabilidad uniforme y la función utilidad exponencial.

En un segundo artículo (Acosta, 2021) utiliza además de la uniforme, las funciones normal y triangular.

Cuando se ha transformado el problema en determinista, se emplea el método ProAct (Hammond et al, 2000) que alterna los análisis de dominancia con los de permutas compensatorias.

En el análisis de dominancia se eliminan todas las opciones dominadas. Se considera que una opción A domina a B cuando todas las medidas de efectividad en A son mejores o iguales que las de B y al menos una de ellas es estrictamente mejor.

Para las permutas compensatorias se le pide al decisor que considere las variaciones en las medidas de efectividad que se deben hacer para que todas las alternativas tengan igual una de esas medidas. En cuanto se logra ello se elimina esa medida de efectividad que es igual para todas las alternativas.

Así, alternando dominancia (para eliminar alternativas) y permutas compensatorias (para eliminar medidas de efectividad) se llega, después de varias iteraciones, a alternativas evaluadas con una sola medida de efectividad. La que tenga el mejor valor en esa medida de efectividad será la mejor opción.

Se presenta a continuación la transformación del problema aleatorio en uno determinista considerando además de la uniforme y la normal, las funciones densidad de probabilidad Cauchy, Chi-cuadrada, Erlang, Gamma y Laplace.

II. TRANSFORMACIÓN DEL PROBLEMA ALEATORIO EN UNO DETERMINISTA

Para esta transformación se calcula, como se mencionó anteriormente, para cada alternativa de decisión i y cada medida de efectividad j, el equivalente bajo certeza, EBC_{ij}, considerando

$u(EBC_{ij}) = \int_{-\infty}^{\infty} f_{ij}(x_0)u_j(x_0)dx_0$ donde $f_{ij}(x_0)$ es la función densidad de probabilidad de la medida de efectividad j cuando se toma la alternativa i; $u_j(x_0)$ es la utilidad del decisor sobre la medida de efectividad j.

Usando la integral anterior, se obtienen las fórmulas que permiten el cálculo de EBC dependiendo de la función densidad de probabilidad, el tipo de comportamiento y si la función utilidad es monotónica creciente o decreciente.

Keeney y Raiffa (1976) establecen que cuando las preferencias son crecientes y se tiene aversión constante al riesgo $u(x_0) = -e^{-cx_0}$ y para propensión constante al riesgo $u(x_0) = e^{cx_0}$; cuando las preferencias son decrecientes y se tiene aversión constante al riesgo $u(x_0) = -e^{cx_0}$ y para propensión constante al riesgo $u(x_0) = e^{-cx_0}$

Por ejemplo, para determinar la fórmula para calcular EBC si las preferencias son crecientes, con propensión constante al riesgo y una función densidad de probabilidad de Laplace,

$$u(EBC) = \int_{x_0=-\infty}^{\infty} f_0(x_0)u(x_0)dx_0 = \int_{x_0=-\infty}^{\infty} \frac{a}{2}e^{-a|x_0-b|}e^{cx_0}dx_0$$

Como se tiene el valor absoluto $|x_0 - b|$, entonces $|x_0 - b| = \{x_0 - b \;\; si\, x_0 \geq b \; b - x_0 \;\; si\, x_0 < b\}$

$$\text{Luego } u(EBC) = \int_{x_0=-\infty}^{b} e^{-a(b-x_0)}e^{(a+c)x_0}dx_0 + \int_{x_0=b}^{\infty} \frac{a}{2}e^{-a(x_0-b)}e^{cx_0}dx_0 =$$

$$= \frac{ae^{-ab}}{2}\int_{x_0=-\infty}^{b} e^{(a+c)x_0}dx_0 + \frac{ae^{ab}}{2}\int_{x_0=b}^{\infty} e^{(-a+c)x_0}dx_0 =$$

$$= \frac{ae^{-ab}}{2(a+c)}e^{(a+c)b} + \frac{ae^{ab}}{2(a-c)}e^{(c-a)b} = \frac{a^2e^{bc}}{a^2-c^2}$$

Como $u(EBC) = e^{cEBC}$ entonces $e^{cEBC} = \frac{a^2e^{bc}}{a^2-c^2}$ empleando el logaritmo natural en ambos lados de la ecuación y despejando EBC, queda $EBC = \frac{1}{c}Ln\left(\frac{a^2e^{bc}}{a^2-c^2}\right)$

La fórmula anterior se colocó en su lugar en la Tabla 2.

De la misma manera se desarrollaron las demás fórmulas que se muestran en las Tablas 1 y 2, donde el de la función uniforme está en el artículo de Acosta (2019) y el de la función normal en el de 2021.

Tabla 1: EBC u(x) creciente y aversión constante al riesgo o u(x) decreciente y propensión

Función de probabilidad	parámetros	rango	EBC
Uniforme, $\frac{1}{b-a}$	a, b, media = $\frac{a+b}{2}$	$a \leq x_0 \leq b$	$\frac{-1}{c}Ln\left\|\frac{e^{-cb}-e^{-ca}}{c(a-b)}\right\|$
Normal $\frac{1}{\sqrt{2\pi}\sigma}e^{\frac{-(x_0-m)^2}{2\sigma^2}}$	Media = m, varianza = σ^2	$-\infty < x_0 < \infty$	$m - \frac{c\sigma^2}{2}$
Exponencial, $\lambda e^{-\lambda x_0}$	Media = $\frac{1}{\lambda}$	$0 \leq x_0$	$\frac{-1}{c}Ln\frac{\lambda}{c+\lambda}$

London Journal of Engineering Research

Cauchy, $\frac{1}{\pi}\frac{a}{a^2+(x_0-b)^2}$	Media = b, $a > 0, \ -\infty < b <$	$-\infty < x_0 < \infty$	b + a
Chi-cuadrada, $\frac{x_0^{\left(\frac{n}{2}-1\right)}e^{\frac{-x_0}{2}}}{2^{\frac{n}{2}}\left(\frac{n}{2}-1\right)!}$	Media = n	$x_0 > 0$	$\frac{-n}{2c}Ln\left(\frac{1}{1+2c}\right)$
Erlang, $\frac{a^n x_0^{n-1} e^{-ax_0}}{(n-1)!}$	Media = $\frac{n}{a}$, $a > 0$	$x_0 > 0$	$\frac{-n}{c}Ln\left(\frac{a}{c+a}\right)$
Gamma, $\frac{x_0^a e^{\frac{-x_0}{b}}}{a!b^{a+1}}$	Media = $(a + 1)b$, $a >- 1, \ b > 0$	$x_0 > 0$	$\frac{-1}{c}Ln\left(\frac{-1}{(1+bc)^{a+1}}\right)$
Laplace, $\frac{a}{2}e^{-a\lvert x_0-b\rvert}$	Media = b, $a > 0$, $-\infty < b < \infty$	$-\infty < x_0 < \infty$	$-\frac{1}{c}Ln\left(\frac{a^2e^{-bc}}{a^2-c^2}\right)$

Tabla 2: EBC u(x) creciente y propensión constante al riesgo o u(x) decreciente y aversión

Función de probabilidad	parámetros	rango	EBC
Uniforme, $\frac{1}{b-a}$	a, b	$a \le x_0 \le b$	$\frac{1}{c}Ln\left\lvert\frac{e^{cb}-e^{ca}}{c(b-a)}\right\rvert$
Normal $\frac{1}{\sqrt{2\pi}\sigma}e^{\frac{-(x_0-m)^2}{2\sigma^2}}$	Media = m, varianza = σ^2	$-\infty < x_0 < \infty$	$m + \frac{c\sigma^2}{2}$
Exponencial, $\lambda e^{-\lambda x_0}$	Media = $\frac{1}{\lambda}$	$0 \le x_0$	$\frac{1}{c}Ln\frac{\lambda}{\lvert c-\lambda\rvert}$
Cauchy, $\frac{1}{\pi}\frac{a}{a^2+(x_0-b)^2}$	Media = b, $a > 0, \ -\infty < b < \infty$	$-\infty < x_0 < \infty$	b-a
Chi-cuadrada, $\frac{x_0^{\left(\frac{n}{2}-1\right)}e^{\frac{-x_0}{2}}}{2^{\frac{n}{2}}\left(\frac{n}{2}-1\right)!}$	Media = n	$x_0 > 0$	$\frac{n}{2c}Ln\left(\frac{1}{2c-1}\right)$
Erlang, $\frac{a^n x_0^{n-1} e^{-ax_0}}{(n-1)!}$	Media = $\frac{n}{a}$, $a > 0$	$x_0 > 0$	$\frac{n}{c}Ln\left(\frac{a}{c-a}\right)$
Gamma, $\frac{x_0^a e^{\frac{-x_0}{b}}}{a!b^{a+1}}$	Media = $(a + 1)b$, $a >- 1, \ b > 0$	$x_0 > 0$	$\frac{1}{c}Ln\left(\frac{1}{(bc-1)^{a+1}}\right)$
Laplace, $\frac{a}{2}e^{-a\lvert x_0-b\rvert}$	Media = b, $a > 0$, $-\infty < b < \infty$	$-\infty < x_0 < \infty$	$\frac{1}{c}Ln\left(\frac{a^2e^{bc}}{a^2-c^2}\right)$

III. MÉTODO PROACT MODIFICADO

El algoritmo propuesto en este artículo consiste en transformar el problema aleatorio en uno determinista y después aplicar el método ProAct modificándolo, mediante la utilización de una función valor de dos atributos en las permutas compensatorias en vez de preguntar directamente al decisor, como sugieren los autores del método. Si la función valor de dos atributos cumple con la condición de intercambios correspondientes es de tipo aditivo, es decir, $v(x_0, y_0) = v_x(x_0) + v_y(y_0)$.

La condición de intercambios correspondientes (Keeney y Raiffa, 1976) consiste en lo siguiente:

Considere cuatro puntos

$$A: (x_1, y_1),\ B: (x_1, y_2),\ C: (x_2, y_1)\ y\ D: (x_2, y_2)$$

Suponga que se cumple lo siguiente:

1. En (x_1, y_1) un aumento b en Y compensa una disminución a en X;
2. En (x_1, y_2) un aumento c en Y compensa una disminución a en X;

3. En (x_2, y_1) un aumento b en Y compensa una disminución d en X;

Si en (x_2, y_2) un aumento c en Y compensa una disminución d en X y esto se cumple independientemente de las cantidades $x_1, x_2, y_1, y_2, a, b, c, d$, se dice que se satisface la condición de intercambios correspondiente.

Keeney y Raiffa (1976) mencionan incluso que la función valor puede utilizarse, por facilidad de análisis, aún cuando sus resultados sean aproximaciones a los reales

También, como los tres axiomas de funciones valor son los tres primeros de los siete de las funciones utilidad (De Neufville, 1990) es posible concluir que todas las funciones utilidad son funciones valor y que no todas las funciones valor son funciones utilidad.

$$\text{Luego, } v(x_0, y_0) = k_1 u_x(x_0) + k_2 u_y(y_0)$$

A continuación, se presenta el algoritmo donde interactúan el decisor y el analista.

Algoritmo

Parte uno: Definición de objetivos, medidas de efectividad y función utilidad

Paso 1-1 El analista le pide al decisor que defina el horizonte de planeación, los objetivos, las medidas de efectividad y sus rangos, estableciendo si las medidas son monotónicas crecientes o decrecientes.

Paso 1-2 El analista para cada medida de efectividad forma la lotería L cuyas consecuencias son los extremos del rango proporcionado en el paso anterior, le asigna probabilidades de 0.5 a cada una y le pregunta al decisor el equivalente bajo certeza (EBC) de cada lotería.

Paso 1-3 El analista calcula el valor esperado (VE) de cada lotería y determina la función utilidad, u(x) de cada medida de efectividad. Como establecen Keeney y Raiffa (1976) si las preferencias son crecientes (por ejemplo, ganancias) entonces, si EBC = VE, neutralidad al riesgo, u(x) = x; si EBC < VE, aversión al riesgo, $u(x) = -e^{-cx}$; si EBC > VE, propensión al riesgo, $u(x) = e^{cx}$; si las preferencias son decrecientes (por ejemplo, costos) entonces, si EBC = VE, neutralidad al riesgo, u(x) = -x; si EBC > VE, aversión al riesgo $u(x) = -e^{cx}$; si EBC < VE, propensión al riesgo, $u(x) = e^{-cx}$

Paso 1-4 El analista, para cada medida de efectividad donde el decisor tiene aversión o propensión al riesgo, determina el valor de c > 0, mediante la ecuación u(EBC) = u(L). Para ello puede utilizar el algoritmo Newton-Raphson, $c_{n+1} = c_n - \frac{f(c)}{f'(c)}$; donde $f(c) = u(L) - u(EBC)\ y\ f'(c)$ es la primera derivada de f con respecto a c

Parte dos: Estipulación de alternativas

Paso 2-1 El analista le pide al decisor que estipule las alternativas, precisando para cada una de ellas la función densidad de probabilidad de cada medida de efectividad, su rango, su media y su desviación estándar.

Paso 2-2 El analista calcula el EBC de cada alternativa y medida de efectividad, utilizando las tablas 1 y 2 cuando el decisor tiene aversión o propensión. En el caso de neutralidad EBC = media de la función densidad de probabilidad. El analista presenta los EBC calculados en una Tabla cuyos renglones son las alternativas y las columnas las medidas de efectividad.

Parte tres: Selección de la mejor alternativa.

Paso 3-1 El analista encuentra y elimina las alternativas dominadas. La alternativa A domina a la B cuando A es mejor que B en algunas medidas de efectividad y en todas los demás es igual que B.

Paso 3-2 El analista ve las alternativas que no han sido eliminadas. Si sólo queda una, esa es la mejor opción y termina el algoritmo. Si no es así, habrá que continuar con el Paso 3-3.

Paso 3-3 El analista le hará una pregunta al decisor para determinar la función valor para dos medidas de efectividad. Sean X, Y dos medidas de efectividad, donde (x_*, y_*) son los peores valores y (x^*, y^*) *son los mejores*. El analista le pregunta la cantidad de x donde $(x, y_*) \sim (x_*, y^*)$. Como hay indiferencia $v(x, y_*) = v(x_*, y^*)$

Si se cumple la condición de intercambios correspondientes la función valor es de tipo aditivo, o sea, $v(x, y) = v_x(x) + v_y(y)$. Como todas las funciones utilidad son funciones valor, se emplean las funciones determinadas en el Paso 1-3.

$$\text{Quedando } v(x, y) = k_x u_x(x) + k_y u_y(y) \text{ y } k_x + k_y = 1; \text{ usando } v(x, y_*) = v(x_*, y^*), \text{ queda}$$

$$k_x u_x(x) + k_y u_y(y_*) = k_x u_x(x_*) + k_y u_y(y^*) \text{ y } k_x + k_y = 1,$$

que es un sistema de dos ecuaciones con dos incógnitas. Al resolver este sistema está determinada la función valor para dos medidas de efectividad.

Si sólo quedan dos medidas de efectividad se evalúan, usando la función valor, todas las alternativas y la que tenga el valor mayor es la mejor opción y termina el algoritmo. Si no es así, habrá que continuar con el Paso 3-4.

Paso 3-4 El analista con la función valor de dos medidas de efectividad, puede hacer que todas las alternativas tengan igual una de esas medidas. En cuanto logra ello se elimina la medida de efectividad que es igual para todas las alternativas, y se regresa al Paso 3-1.

Se presenta ahora un ejemplo donde se aplican los pasos del algoritmo.

IV. EJEMPLO. ELECCIÓN DEL SITIO DONDE SE VA A CONSTRUIR UN AEROPUERTO

Parte uno: Definición de objetivos, medidas de efectividad y función utilidad

Paso 1-1 El analista le pide al decisor que defina el horizonte de planeación, los objetivos, las medidas de efectividad y sus rangos, estableciendo si las preferencias de las medidas son monotónicas crecientes o decrecientes.

El decisor definió como horizonte de planeación 30 años, y cuatro objetivos:

Minimizar el costo de construcción y de operación del aeropuerto. Su medida de efectividad, x_1, es dicho costo en miles de millones de pesos en valor presente; su rango [a, b] = [50, 200] mil millones de pesos; su preferencia es monotónica decreciente.

Minimizar el tiempo de acceso al aeropuerto. Su medida de efectividad, x_2, es el tiempo promedio para llegar al aeropuerto desde diferentes zonas en minutos; su rango [a, b] = [15, 90] minutos; su preferencia es monotónica decreciente.

Maximizar la capacidad del aeropuerto. Su medida, x_3, es el número de despegues y aterrizajes por hora; su rango [a, b] = [50, 250] operaciones por hora; su preferencia es monotónica creciente.

Minimizar el efecto de la contaminación del ruido causado por los aviones. Su medida, x_4, es el número de miles de personas sujetas a un nivel de ruido de 80 decibeles o más; su rango [a, b] = [10, 200] miles de personas; su preferencia es monotónica decreciente.

Paso 1-2 El analista para cada medida de efectividad forma la lotería L cuyas consecuencias son los extremos del rango proporcionado en el paso anterior, le asigna probabilidades de 0.5 a cada extremo y le pregunta al decisor el equivalente bajo certeza (EBC) de cada lotería.

En la Tabla 3 están las respuestas del decisor.

Tabla 3: EBC de la lotería L = [a, 0.5; b, 0.5]

Medida de efectividad	a	b	EBC
x_1: *costo*	50	200	140
x_2: *tiempo de acceso*	15	90	60
x_3: *capacidad*	50	250	120
x_4: *personas afectadas por el ruido*	10	200	120

Paso 1-3 El analista calcula el valor esperado (VE) de cada lotería. Con los valores de EBC y VE, así como el conocimiento si la medida de efectividad es monotónica creciente o decreciente, utilizando las Tablas 1 y 2, determina la función utilidad, u(x). El resultado está en la Tabla 4.

Tabla 4: u(x) para cada medida de efectividad

Medida de efectividad	Lotería	VE	Función monotónica	VE vs EBC	u(x)
x_1	$L(50, 0.5; 200, 0.5)$	125	decreciente	VE<EBC	$-e^{cx}$
x_2	$L(15, 0.5; 90, 0.5)$	52.5	decreciente	VE<EBC	$-e^{cx}$
x_3	$L(50, 0.5; 250, 0.5)$	150	creciente	VE>EBC	$-e^{-cx}$
x_4	$L(10, 0.5; 200, 0.5)$	105	decreciente	VE<EBC	$-e^{cx}$

Paso 1-4 El analista, para cada medida de efectividad donde el decisor tiene aversión o propensión al riesgo, formula la ecuación u(EBC) = u(L), que es una ecuación con una sola incógnita, el parámetro c, y resuelve dicha ecuación. (Puede utilizar el algoritmo Newton-Raphson)

Para la primera medida de efectividad, $-e^{140c} = 0.5\left(-e^{50c}\right) + 0.5(-e^{200c})$

De manera que $f(c) = e^{50c} + e^{200c} - 2e^{140c}$

Su derivada $f'(c) = 50e^{50c} + 200e^{200c} - 280e^{140c}$

Utilizando el algoritmo Newton-Raphson

$$c_{n+1} = c_n - \frac{f(c)}{f'(c)}$$

Proporciona c = 0.00548, luego $u_1\left(x_1\right) = -e^{0.00548x_1}$

Para la segunda medida de efectividad, $-e^{60c} = 0.5\left(-e^{15c}\right) + 0.5(-e^{90c})$

De manera que $f(c) = e^{15c} + e^{90c} - 2e^{60c}$

London Journal of Engineering Research

Su derivada $f'(c) = 15e^{15c} + 90e^{90c} - 120e^{60c}$

Utilizando el algoritmo Newton-Raphson

$$c_{n+1} = c_n - \frac{f(c)}{f'(c)}$$

Proporciona c = 0.01096, luego $u_2(x_2) = -e^{0.01096x_2}$

Para la tercera medida de efectividad, $-e^{-120c} = 0.5(-e^{-50c}) + 0.5(-e^{-250c})$

De manera que $f(c) = e^{-50c} + e^{-250c} - 2e^{-120c}$

Su derivada $f^{'(c)} = -50e^{-50c} - 250e^{-250c} + 240e^{-120c}$

Utilizando el algoritmo Newton-Raphson

$$c_{n+1} = c_n - \frac{f(c)}{f'(c)}$$

Proporciona c = 0.00639, luego $u_3(x_3) = -e^{-0.00639x_3}$

Para la cuarta medida de efectividad, $-e^{120c} = 0.5(-e^{10c}) + 0.5(-e^{200c})$

De manera que $f(c) = e^{10c} + e^{200c} - 2e^{120c}$

Su derivada $f'(c) = 10e^{10c} + 200e^{200c} - 240e^{120c}$

Utilizando el algoritmo Newton-Raphson

$$c_{n+1} = c_n - \frac{f(c)}{f'(c)}$$

Proporciona c = 0.00338, luego $u_4(x_4) = -e^{0.00338x_4}$

Parte dos: Estipulación de alternativas

Paso 2-1 El analista le pide al decisor que estipule las alternativas, precisando para cada una de ellas la función densidad de probabilidad de cada medida de efectividad, su rango, su media y su desviación estándar. Información que se presenta en las Tablas 5 a 8.

Tabla 5: Medida de efectividad 1. Costo (miles de millones de pesos)

Alternativa	Función densidad	Rango		Media	Desviación estándar
		a	b	$m = \frac{a+b}{2}$	$\sigma = \frac{b-a}{\sqrt{12}}$
Sitio 1	Uniforme	50	70	60	5.773503
Sitio 2	Uniforme	60	100	80	11.54701
Sitio 3	Uniforme	80	120	100	11.54701
Sitio 4	Uniforme	100	200	150	28.86751
Sitio 5	Uniforme	60	90	75	8.660254
Sitio 6	Uniforme	90	150	120	17.32051
Sitio 7	Uniforme	130	190	160	17.32051
Sitio 8	Uniforme	120	140	130	5.773503
Sitio 9	Uniforme	130	170	150	11.54701
Sitio 10	Uniforme	150	180	165	8.660254

Tabla 6: Medida de efectividad 2. Tiempo de acceso (minutos)

Alternativa	Función densidad	Rango		Media $m = \frac{a+b}{2}$	Desviación estándar $\sigma = \frac{b-m}{3.6}$
		a	**b**		
Sitio 1	Normal	15	35	25	2.777778
Sitio 2	Normal	35	55	45	2.777778
Sitio 3	Normal	55	75	65	2.777778
Sitio 4	Normal	75	90	82.5	2.083333
Sitio 5	Normal	20	40	30	2.777778
Sitio 6	Normal	40	60	50	2.777778
Sitio 7	Normal	60	80	70	2.777778
Sitio 8	Normal	15	75	45	8.333333
Sitio 9	Normal	35	90	62.5	7.638889
Sitio 10	Normal	20	30	25	1.388889

Tabla 7: Medida de efectividad 3. Capacidad (operaciones por hora)

Alternativa	Función densidad	Rango		Media $m = \frac{a+b}{2}$	Desviación estándar $\sigma = \frac{b-m}{3.6}$
		a	b		
Sitio 1	Normal	50	100	75	6.944444
Sitio 2	Normal	100	150	125	6.944444
Sitio 3	Normal	150	200	175	6.944444
Sitio 4	Normal	200	250	225	6.944444
Sitio 5	Normal	70	120	95	6.944444
Sitio 6	Normal	140	160	150	2.777778
Sitio 7	Normal	180	220	200	5.555556
Sitio 8	Normal	240	250	245	1.388889
Sitio 9	Normal	220	230	225	1.388889
Sitio 10	Normal	200	210	205	1.388889

Tabla 8: Medida de efectividad 4. Personas afectadas por el ruido (miles de personas)

Alternativa	Función densidad	Rango		Media $m = \frac{a+b}{2}$	Desviación estándar $\sigma = \frac{b-m}{3.6}$
		a	b		
Sitio 1	Normal	10	50	30	5.555556
Sitio 2	Normal	50	100	75	6.944444
Sitio 3	Normal	100	150	125	6.944444
Sitio 4	Normal	150	200	175	6.944444
Sitio 5	Normal	40	70	55	4.166667
Sitio 6	Normal	60	110	85	6.944444
Sitio 7	Normal	130	170	150	5.555556
Sitio 8	Normal	30	70	50	5.555556
Sitio 9	Normal	70	120	95	6.944444
Sitio 10	Normal	140	160	150	2.777778

Paso 2-2 El analista calcula el EBC de cada alternativa y medida de efectividad, utilizando las tablas 3 y 4. Y presenta los EBC calculados en una Tabla cuyos renglones son las alternativas y las columnas las medidas de efectividad. El resultado está en la Tabla 9.

Tabla 9: Equivalentes bajo certeza

Alternativas	Costo	Tiempo de acceso	Capacidad	Afectación por ruido
Sitio 1	60.09	25.02	74.85	30.05
Sitio 2	80.37	45.03	124.85	75.08
Sitio 3	100.37	65.03	174.85	125.08
Sitio 4	152.28	82.51	224.85	175.08
Sitio 5	75.21	30.03	94.85	55.03
Sitio 6	120.82	50.03	149.98	85.08
Sitio 7	160.82	70.02	199.90	150.05
Sitio 8	130.09	45.22	244.99	50.05
Sitio 9	150.37	62.69	224.99	95.08
Sitio 10	165.21	25.01	204.99	150.01

Parte tres: Selección de la mejor alternativa

Paso 3-1 El analista encuentra y elimina las alternativas dominadas. La alternativa A domina a la B cuando A es mejor que B en algunas medidas de efectividad y en todas los demás es igual que B.

El sitio 8 domina a los sitios 4 y 7, por lo cual quedan eliminados. Quedando así la Tabla 10.

Tabla 10: Equivalentes bajo certeza

Alternativas	Costo	Tiempo de acceso	Capacidad	Afectación por ruido
Sitio 1	60.09	25.02	74.85	30.05
Sitio 2	80.37	45.03	124.85	75.08
Sitio 3	100.37	65.03	174.85	125.08
Sitio 5	75.21	30.03	94.85	55.03
Sitio 6	120.82	50.03	149.98	85.08
Sitio 8	130.09	45.22	244.99	50.05
Sitio 9	150.37	62.69	224.99	95.08
Sitio 10	165.21	25.01	204.99	150.01

Paso 3-2 El analista ve las alternativas que no han sido eliminadas. Si sólo queda una, esa es la mejor opción y termina el algoritmo. Si no es así, habrá que continuar con el Paso 3-3.

Como aún hay 8 sitios no dominados, se continúa con el Paso 3-3

Paso 3-3 El analista le hará una pregunta al decisor para determinar la función valor para dos medidas de efectividad.

El analista escoge dos medidas de efectividad. En este ejemplo seleccionó x_1: costo con rango [50, 200] y x_2: tiempo de acceso con rango [15,90].

El analista le pregunta al decisor el valor de x_1 que le hace indiferente $(200, 15)$ con $\left(x_1, 90\right)$. El decisor contestó x_1 =100.

Por lo anterior, $v(200, 15) = v(100, 90)$

Como $v\left(x_1, x_2\right) = k_1 u_1\left(x_1\right) + k_2 u_2\left(x_2\right)$ entonces $k_1 u_1(200) + k_2 u_2(15) = k_1 u_1(100) + k_2 u_2(90)$ donde $u_1\left(x_1\right) = -\ e^{0.00548 x_1}$ y $u_2\left(x_2\right) = -\ e^{0.01096 x_2}$ que fueron determinadas en el Paso 1-4.

Esta ecuación junto con $k_1 + k_2 = 1$ constituye un sistema de dos ecuaciones con dos incógnitas, que al resolverlo se tiene $k_1 = 0.543489, k_2 = 0.456511$

Como el número de medidas de efectividad que permanecen es diferente de 2, habrá que continuar con el paso siguiente.

Paso 3-4 El analista con la función valor de dos medidas de efectividad, puede hacer que todas las alternativas tengan igual una de esas medidas. En cuanto se logra ello se elimina la medida de efectividad que es igual para todas las alternativas, y el analista regresa al Paso 3-1.

El analista fijó el tiempo de acceso $x_2^F = 25.02$ minutos y calculó el costo que deben tener las alternativas. Para hacer este cálculo, empleó $(x_1, x_2) \sim (x_1^N, x_2^F)$

Que proporciona $x_1^N = \frac{1}{0.00548} Ln\left(\frac{.543489u_1(x_1)+.456511\left(u_2(x_2)-u_2\left(x_2^F\right)\right)}{0.543489}\right)$

Los costos nuevos, calculados con la fórmula anterior, se muestran en la Tabla 11.

Tabla 11: Nuevos equivalentes bajo certeza

Alternativas	Costo	Tiempo de acceso	Capacidad	Afectación por ruido
Sitio 1	60.09	25.02	74.85	30.05
Sitio 2	109.70	25.02	124.85	75.08
Sitio 3	155.24	25.02	174.85	125.08
Sitio 5	82.58	25.02	94.85	55.03
Sitio 6	150.98	25.02	149.98	85.08
Sitio 8	153.08	25.02	244.99	50.05
Sitio 9	190.75	25.02	224.99	95.08
Sitio 10	165.19	25.02	204.99	150.01

Como todas las alternativas tienen el mismo tiempo de acceso se elimina esa medida de efectividad quedando la Tabla 12.

Tabla 12: Nuevos equivalentes bajo certeza

Alternativas	Costo	Capacidad	Afectación por ruido
Sitio 1	60.09	74.85	30.05
Sitio 2	109.70	124.85	75.08
Sitio 3	155.24	174.85	125.08
Sitio 5	82.58	94.85	55.03
Sitio 6	150.98	149.98	85.08
Sitio 8	153.08	244.99	50.05
Sitio 9	190.75	224.99	95.08
Sitio 10	165.19	204.99	150.01

Se regresa al paso 3-1

Paso 3-1 El analista encuentra y elimina las alternativas dominadas.

El sitio 8 domina a los sitios 9 y 10, por lo que se eliminan los sitios dominados, quedando la Tabla 13.

Tabla 13: Nuevos equivalentes bajo certeza

Alternativas	Costo	Capacidad	Afectación por ruido
Sitio 1	60.09	74.85	30.05
Sitio 2	109.70	124.85	75.08
Sitio 3	155.24	174.85	125.08
Sitio 5	82.58	94.85	55.03
Sitio 6	150.98	149.98	85.08
Sitio 8	153.08	244.99	50.05

Paso 3-2 El analista ve las alternativas que no han sido eliminadas. Si sólo queda una, esa es la mejor opción y termina el algoritmo. Si no es así, habrá que continuar con el Paso 3-3.

Como aún hay 6 sitios no dominados, se continúa con el Paso 3-3

Paso 3-3 El analista le hará una pregunta al decisor para determinar la función valor para dos medidas de efectividad.

El analista escoge dos medidas de efectividad. En este ejemplo seleccionó x_1: costo con rango [50, 200] y x_3: capacidad con rango [50,250] .

El analista le pregunta al decisor el valor de x_1 que le hace indiferente $(200, 250)\ con\ (x_1, 50)$. El decisor contestó x_1 =60.

Por lo anterior, $v(200, 250) = v(60, 50)$

Como $v(x_1, x_3) = k_1 u_1(x_1) + k_3 u_3(x_3)$ entonces $k_1 u_1(200) + k_3 u_3(250) = k_1 u_1(60) + k_3 u_3(50)$ donde $u_1(x_1) = -e^{0.00548 x_1}$ y $u_3(x_3) = -e^{-0.00639 x_3}$ que fueron determinadas en el Paso 1-4.

Esta ecuación junto con $k_1 + k_3 = 1$ constituye un sistema de dos ecuaciones con dos incógnitas, que al resolverlo se tiene $k_1 = 0.246411, k_3 = 0.753589$

$$v(x_1, x_3) = 0.246411\left(-e^{0.00548 x_1}\right) + 0.753589\left(-e^{-0.00639 x_3}\right)$$

Como el número de medidas de efectividad que permanecen es diferente de 2, habrá que continuar con el paso siguiente.

Paso 3-4 El analista con la función valor de dos medidas de efectividad, puede hacer que todas las alternativas tengan igual una de esas medidas. En cuanto se logra ello se elimina la medida de efectividad que es igual para todas las alternativas, y el analista regresa al Paso 3-1.

El analista fijó la capacidad $x_3^F = 244.99$ operaciones por hora y calculó el costo que deben tener las alternativas. Para hacer este cálculo, empleó $(x_1, x_3) \sim (x_1^N, x_3^F)$

Que proporciona $x_1^N = \frac{1}{0.00548} Ln\left(\frac{.246411 u_1(x_1) + .753589\left(u_3(x_3) - u_3\left(x_3^F\right)\right)}{-0.246411}\right)$

Los costos nuevos, calculados con la fórmula anterior, se muestran en la Tabla 14.

Tabla 14: Nuevos equivalentes bajo certeza

Alternativas	Costo	Capacidad	Afectación por ruido
Sitio 1	177.60	244.99	30.05
Sitio 2	171.70	244.99	75.08
Sitio 3	181.44	244.99	125.08
Sitio 5	174.46	244.99	55.03
Sitio 6	189.25	244.99	85.08
Sitio 8	153.08	244.99	50.05

Como todas las alternativas tienen la misma capacidad se elimina esa medida de efectividad quedando la Tabla 15.

Tabla 15: Nuevos equivalentes bajo certeza

Alternativas	Costo	Afectación por ruido
Sitio 1	177.60	30.05
Sitio 2	171.70	75.08
Sitio 3	181.44	125.08
Sitio 5	174.46	55.03
Sitio 6	189.25	85.08
Sitio 8	153.08	50.05

Se regresa al Paso 3-1

Paso 3-1 El analista encuentra y elimina las alternativas dominadas.

El sitio 8 domina a los sitios 2, 3, 5 y 6, por lo que se eliminan los sitios dominados, quedando la Tabla 16.

Tabla 16: Nuevos equivalentes bajo certeza

Alternativas	Costo	Afectación por ruido
Sitio 1	177.60	30.05
Sitio 8	153.08	50.05

Paso 3-2 El analista ve las alternativas que no han sido eliminadas. Si sólo queda una, esa es la mejor opción y termina el algoritmo. Si no es así, habrá que continuar con el Paso 3-3.

Como aún hay 2 sitios no dominados, se continúa con el Paso 3-3

Paso 3-3 El analista le hará una pregunta al decisor para determinar la función valor para dos medidas de efectividad.

Sólo quedan dos medidas de efectividad x_1: costo con rango [50, 200] y x_4: afectación por ruido con rango [10,200] .

El analista le pregunta al decisor el valor de x_1 que le hace indiferente $(200, 10)$ con $(x_1, 200)$. El decisor contestó x_1 =180.

Por lo anterior, $v(200, 10) = v(180, 200)$

Como $v(x_1, x_4) = k_1u_1(x_1) + k_4u_4(x_4)$ entonces $k_1u_1(200) + k_4u_4(10) = k_1u_1(180) + k_4u_4(200)$ donde $u_1(x_1) = -e^{0.00548x_1}$ y $u_4(x_4) = -e^{0.00338x_4}$ que fueron determinadas en el Paso 1-4.

London Journal of Engineering Research

Esta ecuación junto con $k_1 + k_4 = 1$ constituye un sistema de dos ecuaciones con dos incógnitas, que al resolverlo se tiene $k_1 = 0.75, k_4 = 0.25$

$$v(x_1, x_4) = 0.75\left(-e^{0.00548x_1}\right) + 0.25\left(-e^{0.00338x_4}\right)$$

Como sólo quedan dos medidas de efectividad, usando la ecuación anterior, se calcula el valor de los sitios 1 y 8 y se elige el que tenga mayor valor. Así, $v(sitio\ 1) = -2.26$ *y* $v(sitio\ 8) = -2.03$, por lo que el sitio 8 es el mejor.

V. CONCLUSIONES

En este artículo se presenta un algoritmo donde interactúan un decisor y un analista. El analista le hace preguntas al decisor y con sus respuestas efectúa los cálculos requeridos.
El algoritmo siempre converge a una solución óptima.

Los análisis deterministas son más sencillos que los aleatorios, con lo que se logran simplificaciones importantes que permiten llegar a la solución con un esfuerzo mínimo tanto del decisor como del analista.

Este algoritmo es útil cuando existe un solo decisor, una sola etapa y las distribuciones de probabilidad son: uniforme, normal, exponencial, Cauchy, Chi-cuadrada, Erlang, Gamma y Laplace. Si en el problema que se estuviese analizando las distribuciones fuesen diferentes, este artículo presenta el procedimiento para que el analista pueda determinar los valores requeridos de los equivalentes bajo certeza.

REFERENCIAS BIBLIOGRÁFICAS

1. *Acosta Flores José Jesús* (2019) Algoritmo para analizar decisiones con objetivos múltiples bajo incertidumbre. Ingeniería Investigación y Tecnología, volumen XX (numero 1), enero-marzo
2. *Acosta Flores José Jesús* (2021) Algoritmo interactivo para decisiones con varios objetivos, riesgo e incertidumbre. Ingeniería Investigación y Tecnología, volumen XXII (numero 2), abril-junio.
3. *De Neufville Richard* (1990) Applied Systems Analysis: Engineering Planning and Technology Management McGraw-Hill Inc.
4. *Drake Alvin W* (1988) Fundamentals of Applied Probability Theory McGraw-Hill Book Company.
5. *Hammond J. S, Keeney R. L, Raiffa H.* (2000) *Decisiones inteligentes* Gestión 2000.
6. *Keeney Ralph L. and Raiffa Howard* (1976) *Decisions with Multiple Objectives: Preferences and Value Tradeoffs* John Wiley & Sons.
7. *Keeney Ralph L* (1992) *Value-Focused Thinking. A path to Creative Decision making,* Harvard University Press, Cambridge, Massachusetts, USA; London, England.

Study of the Eigenmodes of an Optical Waveguide with a Refractive Index that Varies in the Radial Direction from the Central Axis

Yeong Min Kim

Kyonggi University

ABSTRACT

Finite element analysis has been carried out to investigate the eigenmodes of the optical waveguide whose refractive index varying in radial direction. The cross-section of the waveguide was divided into a mesh of triangle element to perform efficient calculation. The eigenmatrix equation that describe the characteristics of eigenmode was comprised with edges and nodes of triangle elements. Eigenmodes were established with transverse electric field, and electric potential. These eigenmodes were schematically represented with 2-dim electric field, 3-dim electric potential and 2-dim electric equipotential contour. The representations were arranged sequentially from the lower-order eigenmodes. The unusual ones were randomly organized regardless of ordering index to reveal their characteristics more clearly. From the results, it was found that the grad refractive index sufficiently performed the function of focusing electromagnetic waves in the central region.

Keywords: optical waveguide, grad refraction index, triangle element, eigenmatrix equation, electric equipotential contour.

Classification: DDC Code: 621.366

Language: English

LJP Copyright ID: 392952
Print ISSN: 2631-8474
Online ISSN: 2631-8482

London Journal of Engineering Research

Volume 24 | Issue 5 | Compilation 1.0

Study of the Eigenmodes of an Optical Waveguide with a Refractive Index that Varies in the Radial Direction from the Central Axis

Yeong Min Kim

ABSTRACT

Finite element analysis has been carried out to investigate the eigenmodes of the optical waveguide whose refractive index varying in radial direction. The cross-section of the waveguide was divided into a mesh of triangle element to perform efficient calculation. The eigenmatrix equation that describe the characteristics of eigenmode was comprised with edges and nodes of triangle elements. Eigenmodes were established with transverse electric field, and electric potential. These eigenmodes were schematically represented with 2-dim electric field, 3-dim electric potential and 2-dim electric equipotential contour. The representations were arranged sequentially from the lower-order eigenmodes. The unusual ones were randomly organized regardless of ordering index to reveal their characteristics more clearly. From the results, it was found that the grad refractive index sufficiently performed the function of focusing electromagnetic waves in the central region.

Keyword: optical waveguide, grad refraction index, triangle element, eigenmatrix equation, electric equipotential contour.

Author: Kyonggi University, Korea.

I. INTRODUCTION

Previously, we have studied eigenmodes established in the optical waveguides of various types using FEM (Finite Element Method) [1][2]. We also discussed the eigenmodes generated in multiple photonic crystal waveguides [3][4]. In the studies, air or dielectric holes were arranged symmetrically according to the geometry of the photonic crystal waveguide. It would be well known that photonic crystals can confine electromagnetic waves to a specific region and being able to control eigenmodes according to the spatial arrangement of dielectric holes. The refractive indices of these studies mainly were distributed step like. In general, the established eigenmode in the waveguide and the photonic crystal fiber reflect spatial distribution of the refraction index. From these studies, we had identified that they showed unique characteristics of eigenmode in an orderly and consistent manner. Optical fibers with stepped refraction are suitable only for data link of short range. Because the propagation power loss is not negligently slightly. The power loss is due to slightly difference of path shift between the neighbor electromagnetic waves which cause interference and distortion of the information.

The waveguide with multimode graded index is designed to overcome these shortcomings and propagate electromagnetic signals through long distances. This waveguide utilizes the Snell principle, which states that the more considerable refractive index, the smaller the angle of refraction. The refraction value is high at the centre, and decreased as going to clad gradually. Therefore, the destructive interference of electromagnetic waves is weakened and they can be concentrated at one point on the central axis and propagate long distances. This concept was attended from the long time ago and is already being applied in the varied areas [5]. However, only a few analytical solutions for the eigenmodes generated in this waveguide have been presented. As the refractive index changed in the waveguide, solving the Helmholtz equation becomes to be more complicated. To obtain a solution by applying this equation to a realistic physical system, constrained conditions must be imposed

on the problem and satisfied only with an approximate result. At present, to know the properties of the eigenmode of a graded refractive waveguide, its characteristics must be understood through numerical analysis such as FEM etc.

In this study, FEM is carried out to investigate the eigen properties of the multimode coaxial optical waveguide with graded refractive index. To facilitate for calculation of FEM, the cross-section of waveguide is decomposed into a mesh of triangle elements. The Helmholtz equation, which describes the eigenmodes of the waveguide, consists of the edges and nodes of these triangle elements. The solution to this equation is expressed as an edge vector describing the electric field at the center of the triangle, and the value of each node representing the electric potential at any element's position. The eigen equations are proportional to the number of triangle elements of the mesh. To increase the eigenmode resolution, the density of triangle elements must be increased. Then, the size of the eigen equation become more increased and a computer with more significant calculating capacity is needed. However, because the capacity of personal computers is limited, it isn't easy to handle the inverse matrix of the large-size eigen equation. To overcome this contradiction, FEM uses the Arnoldi algorithm to compress the matrix equation into the smaller one, as mentioned in the previous manuscript. Afterwards, the Krylov-Schur iteration method is used to find several prominent eigenmodes with the highest reliability [6][7]. This method is used in this study to find the desired several eigenmodes.

Eigenmodes consist of electric fields and potential pairs. These constitute the column matrix of the similarity transformation matrix used in the iterative method. The mathematical derivation process for FEM has been mentioned in a previous manuscript [1][2]. Therefore, this process is not mentioned again in this manuscript. In other words, the theory of FEM is omitted in this manuscript. The description format of this manuscript deviates from the existing order and is described as follows. This manuscript describes the structure of waveguide, the result and discussion, and conclusion in order.

II. THE STRUCTURE OF THE WAVEGUIDE AND THE SIMILARITY TRANSFORM MATRIX

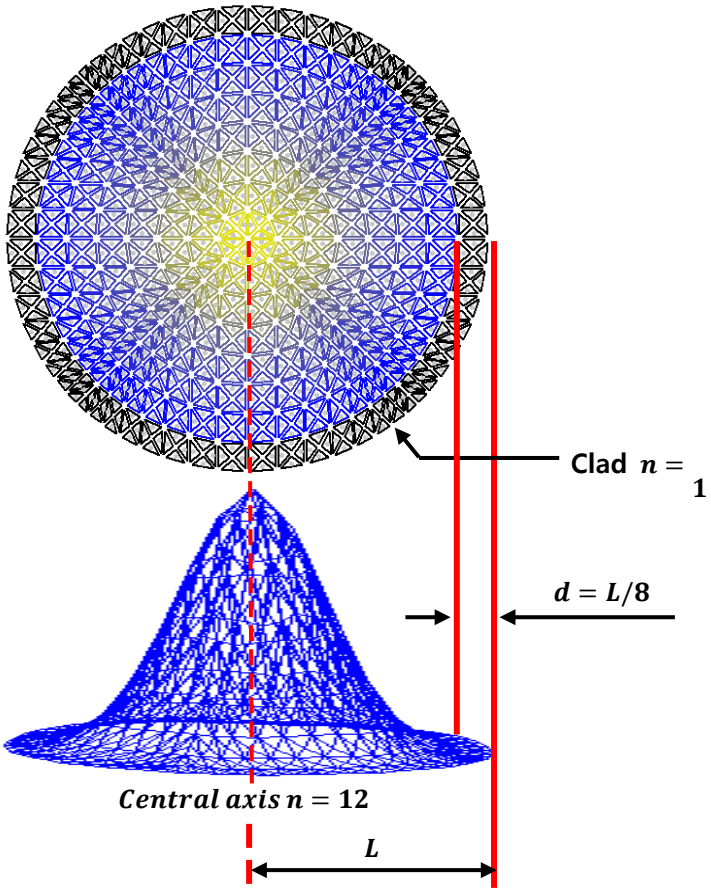

As mentioned in the introduction, a factor that made a significant influenced on the eigenmode establishment in a waveguide is the refractive index in the direction perpendicular to that of electromagnetic wave propagation. The coaxial waveguide used in this study has a structure that gradually changes the refractive index of the core inside the clad through which electromagnetic waves propagate. As shown in Figure 1, the refractive index has a value of 1.0 at the clad and gradually increases up to 12.0 as it approaches the central axis. As the refractive index of the medium increases, the speed of electromagnetic waves is lower than in a vacuum, so the path it travels here is relatively small. Conversely, in places where the refractive index is smaller, the speed of light propagation is relatively faster so that more length it travels at the same amount of time. If the refractive index is increased gradually as approaching to the center, the destructive interference of monochromatic light which incident on the cross-section of the waveguide becomes smaller. Therefore, it is easier to focusing electromagnetic waves on the central axis.

In this study, the refractive index is designed to achieve a spatial distribution of cylindrical symmetry by reflecting the geometric characteristics of the waveguide as much as possible. Therefore, it is expected to act as a positive factor in forming the eigenmode of the multimode-graded refractive index waveguide and improve the resolution of the spectrum. The cross-section of the waveguide is divided as a mesh structure composed of triangle elements, as shown in Figure 1. The refractive indices corresponding to the triangle elements are shown in yellow for the cylindrical central part, blue for the outer part of the core, and black for the inside of the cladding, indicating sequentially the relative magnitudes of the refractive indices.

The edges and nodes of a triangle are essential elements of the eigenmatrix equation. The Helmholtz matrix equation, which describes the eigenmodes formed in the waveguide, consists of a vector component of the edge that represents the electric field and a nodal scalar element that defines the electric potential. The eigenmode is obtained by diagonalizing the matrix equation through similarity transformation. The diagonal components of the resulting Schur matrix represent eigenvalues. However, in this study, to obtain the most ideal shape of the eigenmode, the geometric size of the waveguide was changed and the refractive index was adjusted accordingly.

Therefore, as eigenvalues are not always the same in each calculation, these values are excluded from the results and discussion. The column component of the similarity transformation matrix consists of vector edges and scalar nodes related to electric field and electric potential values, respectively. The electric field is expressed at the barycentric point by combining the edge components of the triangle element, which are vector components. The equipotential contour is obtained by combining the nodal components of the triangle elements. The values at the nodes are combined to find at the point on each edge, and connecting them with to depict the equipotential line. In this study, the eigenmodes are represented as schematically of 2-dim electric field, 3-dim electric potential and 2-dim electric equipotential contours results.

The eigenmode is calculated by dividing the matrix equation into TM (Transverse Magnetic) and TE (Transverse Electric) modes. In FEM calculations, TM and TE modes are distinguished by boundary conditions set on the surface of the waveguide. In this study, it is assumed that the surface of waveguide is a PEC (Perfect Electric Conducting) boundary. In this case, the electric field calculation of TM mode is performed by applying Dirichlet boundary conditions to the. In other word, when obtaining the electric field of TM mode, the calculation is performed by canceling the components of edges and nodes on the surface of the waveguide from the eigenequation. As mentioned in the previous study, the eigenmodes are expressed only as an electric field of TM mode. Because in FEM calculations the magnetic field is obtained through the same process as in the electric field. Then, the eigenequations are reduced by their number, allowing only the tangential component of the electric field and excluding the perpendicular component. The resulting electric

fields and potentials for each mode are subdivided and shown with the schematic representations.

III. RESULT AND DISCUSSION

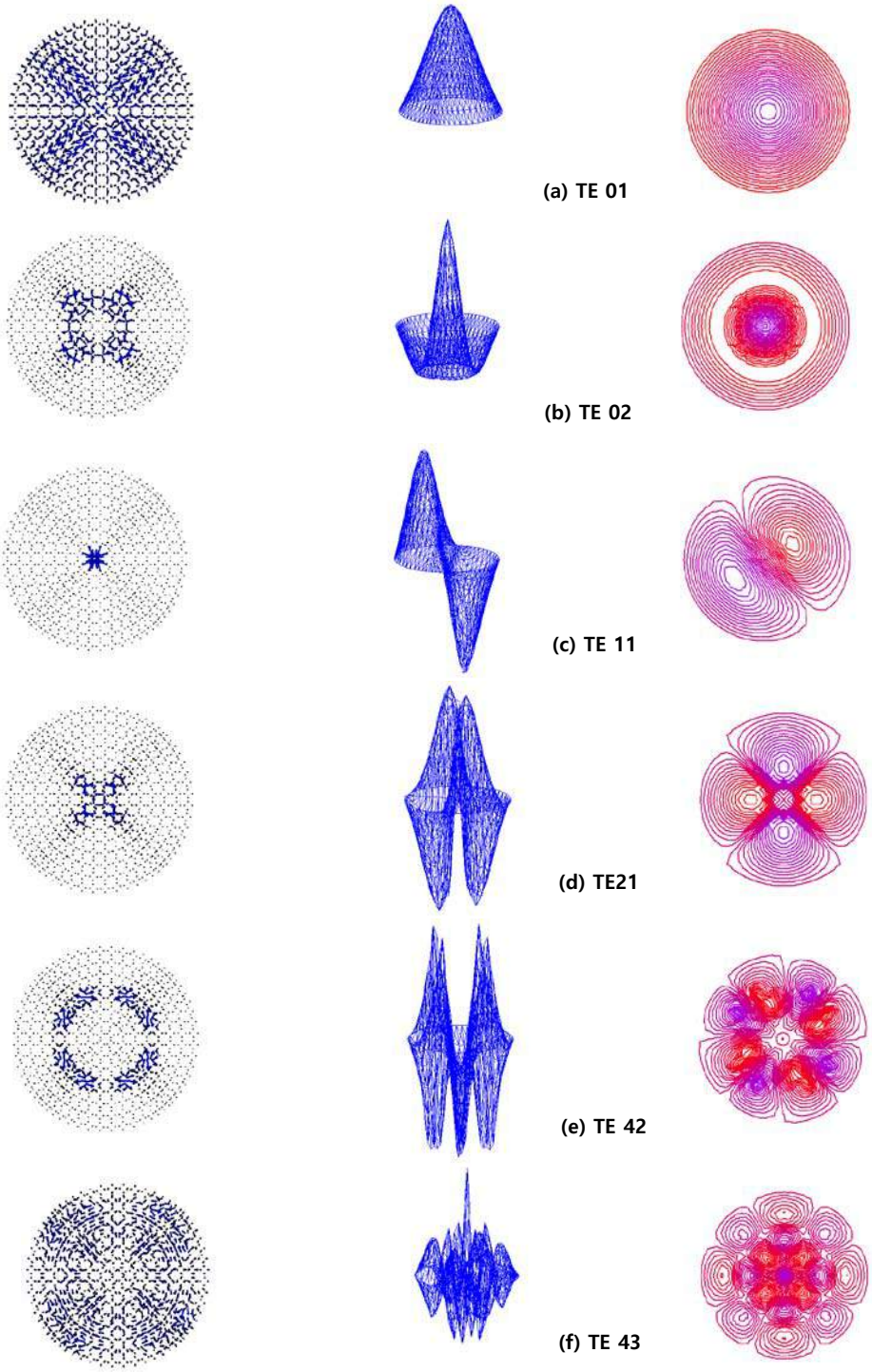

Figure 2: The Schematic Representation of TE Eigenmodes

Figure 2 shows a schematic representation of the TE eigenmodes. These were selected as the eigenmodes of the highest resolution possible.

They were sequentially arranged from the lowest to the highest order eigenmodes. Physical analysis of eigenmodes achieved through electric fields or potentials. As can be seen above, the representation of electric potential is generally more explicit than that of the electric field, and its characteristics can be manifestly discussed. TE and TM modes are distinguished by whether or not the surface of the waveguide is considered PEC during the process of FEM calculation. If the calculation is performed with excluding the surface component, the result with its tangential component of electric field removed is obtained. The electric field component is obtained by taking the spatial gradient of the electric potential.

Figure 2 is the eigenmodes generated in the waveguide expressed as 2-dim electric field, 3-dim electric potential, and 2-dim electric equipotential contours. The 2-dim equipotential contours shown in Figure 2 all take the form parallel to the surface of the waveguide. Their spatial gradient relative to the equipotential contour represents the electric field perpendicular to the surface and describes a typical TE mode. In describing the eigen properties of a waveguide, the electric potential and equipotential contours have a precise shape, but the electric field does not. Therefore, the physical understanding of eigenmodes is achieved through the above two representation, and the electric field is only auxiliary.

Figure 2(a) shows that, according to the spatial distribution of the refractive index, the eigenmode spreads out symmetrically around the circular waveguide. The 3-dim expression for electric potential shows the most incredible intensity at the centre, and the value decreases toward the outskirts, forming a bell shape. This form is presented the most stable eigenmode. And is expected to be able to propagate long range with the reliable and robust property. In the field of optical communications, this eigenmode is used to transmit and receive high energy signal. Unless there is a particular purpose, this eigenmode will be the most preferred waveform in this field. For this spectrum, the eigenmode of TE 01 is imposed in this study. When real-world optical waveguide is made, the surface is not made of PEC. Hence, the tangential electric field is not zero, and energy can dissipate out the waveguide surface. It has been well known that TE 01 mode of a circular waveguide is the lowest of power loss due to symmetry.

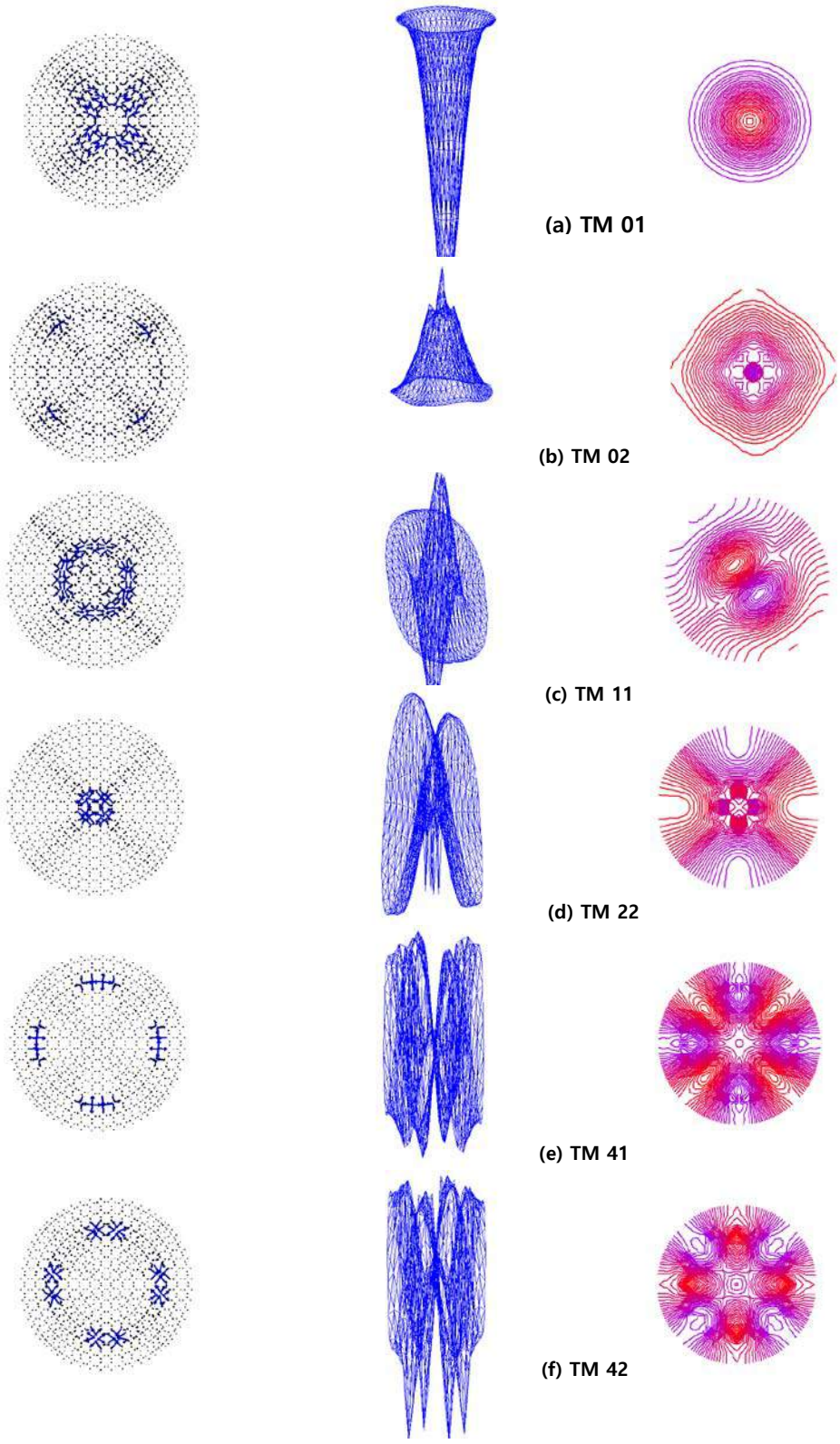

Figure 3: The Schematic Representation of TM Eigenmodes

As the ordering of the mode is increased, the shape of the eigenmodes is more complexed. But some degree of systematicity can be found among them. Figure 2(b) shows eigenmodes represented by two discontinuous concentric circles while maintaining circular symmetry. The 3-dim

eigenmode for electric potential shows the most incredible intensity at the centre, like TE 01 mode. And although the potential value decreases toward the outskirts, the wave disappears at a specific location between the centre and the clad and then increases again. Since there is no discontinuity in the azimuth direction and circular symmetry is maintained, the eigenmode of this spectrum can be named TE 02. Eigenmode TE 02 can also perform an excellent function in transporting information or power. However, in practical applications, mode filters enhance the TE 01 eigenmode and impede the guidance of other modes [8][9]. As the ordering of the mode increases, the azimuth components appear, and the eigenmodes become more complex. Among these, the simplest and most likely eigenmode is TE 11. They appear symmetrically ordered around the waveguide axis. Nevertheless, in reality, they are not used. In this study, these spectra were investigated to identify the diversity of eigenmodes depending on refractive indices.

Figure 3 is a schematic representation of the eigenmodes of TM modes. As like shown in Figure 2, the resolution of electric potential for the eigenmode is more than that of electric field. Therefore, analysis and understanding of eigenmodes are based on the 3-dim electric potential and 2-dim equipotential contours. The electric field only plays an auxiliary role as like TE mode. The electric field describing the TM mode, unlike the TE mode, forms only a tangential component parallel to the surface of the waveguide. As can be seen in the figure, since the electric potential represents only the component perpendicular to the surface, the spatial gradient for it represents the tangential component of the electric field.

Figure 3(a) is a schematic representation of the eigenmode TM 01. Compared to the shape in Figure 3(a), the difference is clearly identified in the 3-dim electric potential image. First of all, the intensity of the TM 01 eigenmode is much greater than that of TE 01. The TM 01 component of the electric potential formed on the surface of the optical waveguide reflects the refractive index well compared to the TE 01. This eigenmode, like that of TE 01, can easily transmit signals or power with little energy loss. The surface of the optical waveguide is assumed to be coated with PEC. The edges and nodes on the surface are omitted in the calculation of FEM for TE mode. In the case of TE mode, a tangential electric field does not appear on the surface, and only a tangential component of the electric potential is exhibited. However, in the case of TM mode, the tangential component of the electric field appears on the surface, and the perpendicular component of the electric potential is exhibited. Near the extended rim, including the surface of the optical waveguide, components of the eigenmode electric field and potential appear.

When comparing the 3-dim electrical potentials, the surface components in Figures 2 and 3 clearly distinguish the characteristics of TE and TM. As the ordering of modes is increased, like does the TE mode, azimuth components appeared and the eigenmodes become more complexed. In Figure 3(b), the eigenmode is named TM 02, and the electric potential at the surface is transformed from a circularly symmetrical structure, and the vertical component appears to it weakly. The electric field that appears along with this is so complex that the eigenmode cannot be determined by itself. This type of phenomenon occurs when the refractive index of the waveguide is not uniform and changes in the space [10]. The refractive index plays a role in concentrating electromagnetic waves in a particular area, but at the same time, it also takes on the complexity of the eigenmode. The following spectrum includes both azimuth and radial components in the core region of waveguide. From its shape, the eigenmode can be determined as TM 11. Compared to TE 11, the vertical component of the potential at the surface is evident, allowing the action of PEC to be confirmed. Changes in refractive index and the presence of PEC add complexity to eigenmode generation in optical waveguides. As for the remaining eigenmodes, the azimuth and radial components increase as in TM 21, promoting spectrum diversity. They exhibit the characteristics of a multi-graded refractive optical waveguide, but if they coexist with the TM 01 mode, they must be quenched through a mode filter. Otherwise, it will act as noise that infringes on the primary signal, such as TM 01.

VI. CONCLUSION

The eigenmodes for the graded refractive optical waveguide were investigated by FEM. The eigenmodes were divided into TE and TM modes and shown in a schematic representation. The eigenmodes TE and TM were identified based on the 2-dim electric equipotential contour, which is determined through the eigen characteristics to the surface of the optical waveguide. The electric equipotential contours were dominated by the tangential component to the surface for the TE mode and the perpendicular one for the TM mode. Among those spectra, the propagation characteristics of the electromagnetic wave in the optical waveguide were discussed through TE 01 and TM 01 eigenmodes.

REFERENCE

1. Yeong Min Kim, "A Study on the Fine Eigenmodes in the Core Region of Coaxial Waveguide Induced by the Dielectric Cladding", Global Journal of Engineering Science and Researches, July 2016, 3(7).
2. Yeong Min Kim, "A Study on the Eigen Properties of the Coaxial Waveguide of Cylindrical Form", Transactions on Engineering and Computing Sciences, Oct., 25, 2023, 11(5).
3. Yeong Min Kim, "A Study on the Contribution of a Buffer Coated with a Perfect Conductor to Constructing Eigenmodes in Square HAPCF", Journal of Electrical and Electronic Engineering, March 2019, 7(1), pp 36- 41.
4. Yeong Min Kim, Se Jung Oh," 홀-보조 광-결정 도파관에 형성된 고유-특성 (The Eigen-Properties Constructed in the HAPCF)", Asia-pacific Journal of Multimedia Services Convergent with Art, Humanities, and Sociology Vol.8, No.11, November (2018), pp. 223-233
5. HECHT," OPTICS 2nd Edit.", ADDISON-WESLEY PUBLISHING COMPANY, 1987, pp 170-176.
6. V. Hernandez, J. E. Roman, A. Tomas, V. Vidal, Krylov-Schur Methods in SLEPc, June, 2007, Available at Available at http://www.grycap.upv.es/slepc.
7. C. J. Reddy, Manohar D. Deshpande, C. R. Cockrell, and Fred B. Beck, NASA Technical Paper, 1994, 3485.
8. W.C. Chew and D. Jiao, "https://engineering.purdue.edu/wcchew/ece604f18/latex%20lecture%20notes/LectureNotes19.pdf", November 13, 2018.
9. Alex Lapidus, "Circuit Simulation of Dual-mode Waveguide Cavity Filters", MicrowaveJournal.com, November 17, 2008.
10. Yeong Min Kim, "A Study on the Fine Eigenmodes in the Core Region of Coaxial Waveguide Induced by the Dielectric Cladding", Transactions on Engineering and Computing Sciences, Dec., 25, 2023, 11(6).

Optimization of Solar Energy using Artificial Neural Network VS Recurrent Neural Network Controller with Ultra Lift Luo Converter

Kasim Ali Mohammad & Sarhan M. Musa

Prairie View A&M University

ABSTRACT

In today's society, the demand for clean energy is essential. Traditionally, renewable sources such as hydropower, wind, and solar have provided sustainable solutions. Photovoltaic (PV) systems generate electricity from sunlight using semiconductor PV cells, which have been effective for over 30 years. The efficiency of PV cells depends on irradiance (solar photon intensity) and temperature. Higher irradiance boosts efficiency, while higher temperatures reduce it. Despite their low voltage outputs, PV systems can be optimized with DC-DC Ultra Lift Luo converters to meet load requirements, improving system efficiency. The Ultra Lift Luo converter, a type of DC-DC converter, offers a higher voltage conversion gain than conventional boost converters. This converter belongs to the Luo converter family, which uses advanced techniques to achieve high voltage gain and efficiency. Solar irradiance fluctuates throughout the day, impacting PV cell output. Maximum Power Point Trackers (MPPTs) adjust the system's operating point to sustain peak efficiency.

Keywords: artificial neural network, dc-dc ultra lift luo converter, maximum power point tracking, photovoltaic system, recurrent neural network.

Classification: DDC Code: 621.47

Language: English

Great Britain Journals Press

LJP Copyright ID: 392953
Print ISSN: 2631-8474
Online ISSN: 2631-8482

London Journal of Engineering Research

Volume 24 | Issue 5 | Compilation 1.0

Optimization of Solar Energy using Artificial Neural Network VS Recurrent Neural Network Controller with Ultra Lift Luo Converter

Kasim Ali Mohammad[α] & Sarhan M. Musa[σ]

ABSTRACT

In today's society, the demand for clean energy is essential. Traditionally, renewable sources such as hydropower, wind, and solar have provided sustainable solutions. Photovoltaic (PV) systems generate electricity from sunlight using semiconductor PV cells, which have been effective for over 30 years. The efficiency of PV cells depends on irradiance (solar photon intensity) and temperature. Higher irradiance boosts efficiency, while higher temperatures reduce it. Despite their low voltage outputs, PV systems can be optimized with DC-DC Ultra Lift Luo converters to meet load requirements, improving system efficiency. The Ultra Lift Luo converter, a type of DC-DC converter, offers a higher voltage conversion gain than conventional boost converters. This converter belongs to the Luo converter family, which uses advanced techniques to achieve high voltage gain and efficiency. Solar irradiance fluctuates throughout the day, impacting PV cell output. Maximum Power Point Trackers (MPPTs) adjust the system's operating point to sustain peak efficiency. This study aims to design AI controllers for MPPT management. In addition, we evaluate the performance of Artificial Neural Networks (ANN) and Recurrent Neural Networks (RNN) with three datasets to determine the most efficient AI controller for optimizing solar energy systems.

Keywords: artificial neural network, dc-dc ultra lift luo converter, maximum power point tracking, photovoltaic system, recurrent neural network.

Author α: Department of Electrical and Computer Engineering, Prairie View A&M University, Prairie View, TX, USA.

σ: Department of Electrical and Computer Engineering, Prairie View A&M University, Prairie View, TX, USA.

I. INTRODUCTION

Historically, energy production mainly involved burning fossil fuels like coal, oil, and natural gas. This process converted their chemical energy into heat, which was then used to generate electricity through various methods. Unfortunately, relying on fossil fuels has significantly increased harmful greenhouse gas emissions, particularly carbon dioxide, over the past 70 years, worsening global climate change. To reduce these environmental impacts, there is a growing movement towards cleaner and more efficient energy conversion methods, especially photovoltaic (PV) systems [1-2].

PV systems convert sunlight directly into electricity using PV cells. However, the voltage output from PV cells is usually low, requiring DC-DC converters to boost the voltage levels. The DC-DC Ultra Lift Luo converter is crucial in this context. This converter not only increases the voltage output but also matches the impedance between the PV system and its connected load, addressing a key challenge in optimizing PV system efficiency [3].

Solar irradiance, which measures the intensity of sunlight photons, varies throughout the day. At the same time, ambient temperature changes based on environmental conditions, affecting the PV system's performance. To maximize energy capture and efficiency, a Maximum Power Point Tracker (MPPT) is used. The MPPT adjusts the PV system's operating point in real-time to ensure it operates at its maximum power point (MPP), where the output power is optimized. This adjustment is critical as it aligns with the varying

maximum voltage curve of the PV cells throughout the day. The MPPT signal guides the DC-DC Ultra Lift Luo converter, which uses components like Insulated Gate Bipolar Transistor (IGBT) diodes to control its duty cycle. By modulating the duty cycle, the converter adjusts the output voltage to match the load requirements effectively [4].

Given the non-linear and dynamic nature of solar irradiance (G) and temperature (T), traditional time-domain controllers may not efficiently manage these variations. Therefore, artificial intelligence (AI) controllers offer a more effective solution. This study considers two AI controller methods: Artificial Neural Networks (ANN) and Recurrent Neural Networks (RNN). These AI controllers excel in handling non-linear changes in input values from PV cells, optimizing control efficiency, and enhancing overall system performance [5-7].

The shift from fossil fuel-based energy generation to renewable sources like PV systems represents a significant step towards sustainability. By integrating advanced technologies such as MPPTs, DC-DC converters, and AI controllers, we can effectively harness solar energy while maximizing efficiency and minimizing environmental impact.

This paper is structures as: Section II: PV System Description and Modeling

- Detailed description of the modeled 213.15-Watt PV array.
- Explanation of the basic block model of PV arrays.
- Discussion on the construction and operation of solar cells based on p-n semiconductor junctions.
- Inputs (G and T) and outputs (voltage output and power output) of the PV array model.
- Methods used for simulating and characterizing the PV system under different conditions.
- DC – DC Ultra Lift Luo Converter Design and Model.

Section III: Methodology of ANN Controller

- Introduction to artificial intelligence (AI) controllers.
- Description of Artificial Neural Network (ANN) model used.
- Explanation of how this AI ANN controller is implemented for optimizing the PV system, particularly focusing on its ability to handle non-linear and dynamic inputs (G and T).

Section IV: Methodology of RNN Controller

- Introduction to artificial intelligence (AI) controllers.
- Description of Recurrent Neural Network (RNN) model used.
- Explanation of how this AI RNN controller is implemented for optimizing the PV system, particularly focusing on its ability to handle non-linear and dynamic inputs (G and T).

Section V: Results and Discussion

- Presentation of the results obtained from the ANN and RNN controllers.
- Comparative analysis of the performance of ANN and RNN in optimizing the PV systems.
- Discussion on the strengths and weaknesses of each AI controller method.
- Interpretation of the results in relation to the efficiency and effectiveness of PV system optimization.

Section V: Conclusion

- Summary of the key findings from the study.
- Contributions to the field of renewable energy and PV system optimization.
- Recommendations for future research directions.
- Closing remarks on the potential impact of using AI controllers in enhancing PV system performance.

II. SYSTEM DESCRIPTION AND MODELING

We present a comprehensive description of the PV system model, detailing its components and the integration of ANN and RNN controllers. Block diagrams are included to illustrate the proposed models. The PV array model receives inputs of Solar Irradiance (G) and Temperature (T) and has two outputs for the ANN controller: Output Voltage and Output Power, and one output for the

RNN controller: Output Voltage. A DC-DC Ultra Lift Luo Converter is employed, with the MPPT playing a crucial role in maximizing power output by adjusting the operating point. The reference voltage (Vpv) is generated based on calculations and predictions from ANN or RNN algorithms. The PV system is directly connected to a fixed load. The block diagrams in Fig. 1 and Fig. 2 visually clarify the system's architecture and control flow [8-10].

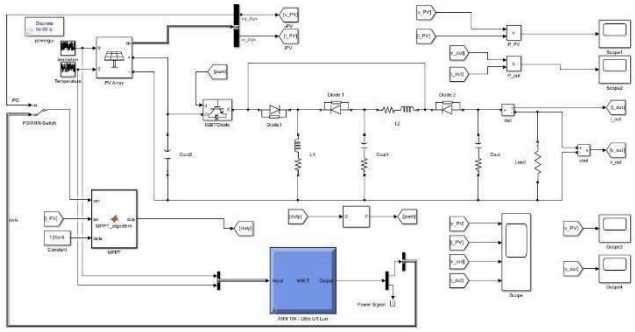

Fig. 1: Block diagram for the proposed designed ANN model

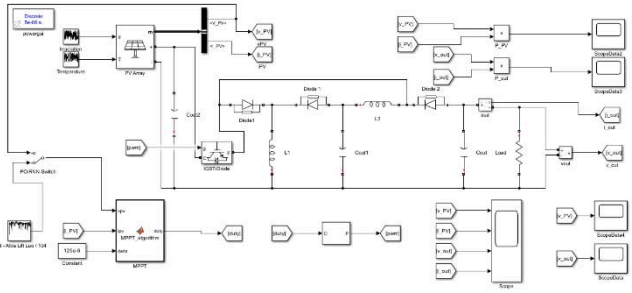

Fig. 2: Block diagram for the proposed designed RNN model

2.1 Mathematical Solar Array Modeling

The single-diode model is commonly used for simulating photovoltaic (PV) cells. This model includes the following components:

1. Photo-current source (I_{ph}): Represents the current generated by the solar cell when exposed to sunlight.
2. Diode (D): Models the p-n junction of the solar cell, providing a path for the recombination of charge carriers.
3. Series Resistance (R_s): Represents the resistive losses within the cell.
4. Shunt Resistance (R_{sh}): Represents leakage currents within the cell.

The equivalent circuit of a PV cell using the single-diode model can be represented as:

$$I = I_{ph} - I_D - I_{sh} \quad (1)$$

Where:

- I is the output current of the PV cell.
- I_{ph} is the photo-generated current.
- I_D is the current through the diode.
- I_{sh} is the shunt leakage current.

In this research, we concentrate on the design and modeling of a 213.15-Watt photovoltaic (PV) array, a critical component for solar energy systems. The PV array is made up of interconnected solar cells that convert sunlight directly into electricity. The main inputs for the array are solar irradiance (G) and temperature (T). Solar irradiance, which measures the intensity of sunlight falling on the PV array in watts per square meter (W/m^2), leads to higher photo-generated current with increased irradiance. Temperature, measured in degrees Celsius (°C), represents the surrounding ambient temperature and impacts the efficiency and output of the PV cells, with higher temperatures typically reducing efficiency. The key outputs of the PV array include the voltage output (V), representing the electrical voltage produced and influenced by both irradiance and temperature, and the power output (P) for the ANN controller, indicating the total electrical power generated by the PV array, calculated as the product of the voltage and current produced by the PV cells [11-13].

Understanding how the PV array operates across different levels of solar irradiance and temperature is essential to gauge its performance capabilities. Through simulating the PV array model in diverse environmental scenarios, we can anticipate its responses and refine its design to achieve optimal efficiency [14].

This research centers on intricately modeling a 213.15-Watt PV array, highlighting its fabrication using p-n semiconductor junctions and its responsiveness to solar irradiance and temperature changes. The voltage and power

outputs serve as key indicators of the PV array's operational efficiency, pivotal for its integration into renewable energy setups. Precise modeling facilitates AI-driven predictions and improvements in the PV array's performance across diverse environmental settings [15].

2.2 Modeling and Simulation of 213.15W PV Array

The photovoltaic (PV) array used in the designed PV system was carefully selected from the MATLAB/Simulink toolbox for simulation purposes. This selection provides detailed information about the array's electrical properties and includes visual aids demonstrating its performance under different temperature and irradiance conditions. Fig. 3 displays a graphical representation of the chosen PV array model from MATLAB/Simulink, illustrating its response to varying environmental factors. Additionally, Table I outlines specific electrical parameters that characterize the PV array, offering a clear understanding of its capabilities and performance metrics under diverse operational scenarios [16-17].

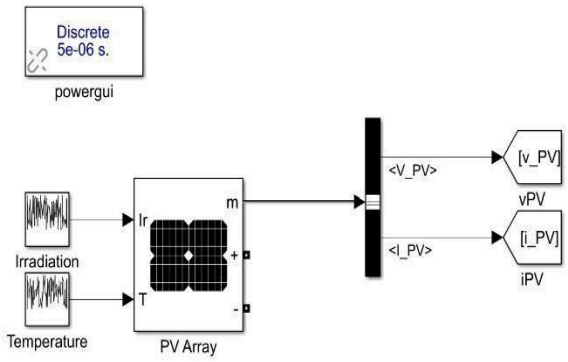

Fig. 3: Block diagram for the proposed designed PV Array model

Table I: Electrical Characteristics Of The Pv Module

Description	User-defined
Maximum power	312.15 W
Voltage at Pmax (Vmax)	29.00V
Current at Pmax (I_m)	7.35 A
Short Circuit current (I_{sc})	7.84 A
Open circuit voltage	36.30 V
Temperature coefficient Ki	0.102 A/°C

The Voltage-Current (V-I) characteristics curve demonstrates how the voltage and current output of the PV array relate to each other under specified conditions, shown in Fig. 4. At a temperature of 25 °C, this curve indicates that the current output remains stable until the voltage approaches a certain threshold (close to the open circuit voltage), beyond which the current decreases significantly [18].

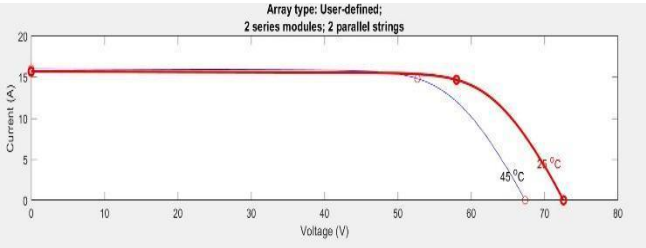

Fig. 4: V-I characteristics curves of the PV array at a specified temperature

The Voltage Power (V-P) characteristics curve illustrates how the power output of the PV array changes with varying voltage levels, specifically at temperatures of 25 °C and 45 °C, as depicted in Fig. 5. Typically, this curve exhibits a peak that signifies the maximum power point (MPP), where the PV array operates most efficiently. Beyond this point, the power output declines as the voltage continues to increase [19-20].

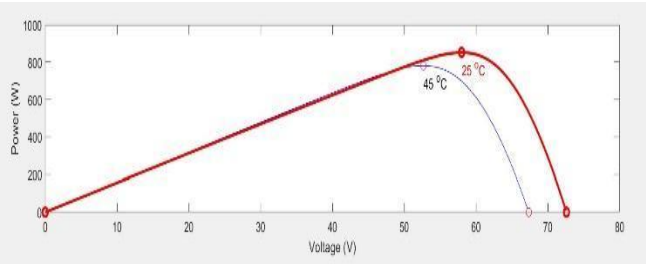

Fig. 5: V-P characteristics curves of the PV array at a specified temperature

The Voltage Current (V-I) characteristics curve, depicted in Fig. 6, illustrates how the output current of the PV array changes with varying voltages under different levels of sunlight intensity. Higher levels of irradiance generally result in increased current outputs, while the overall shape of the curve remains consistent across varying irradiance levels.

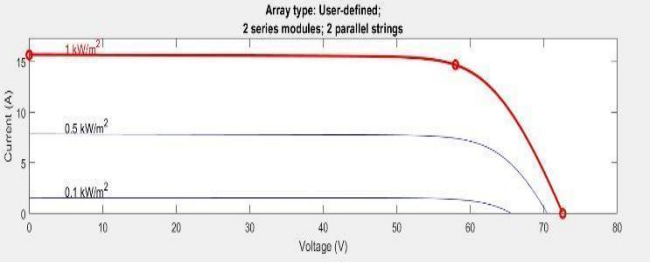

Fig. 6: V-I characteristics curves of the PV array at a specified irradiance

The Voltage Power (V-P) characteristics curve for specified irradiance levels illustrates how the power output changes with voltage under varying sunlight intensities. Like the temperature-dependent V-P curve shown in Fig. 7, the curve influenced by irradiance also exhibits a peak at the maximum power point. Higher irradiance levels lead to higher peak power values, highlighting the direct relationship between sunlight intensity and PV array performance in generating electrical power.

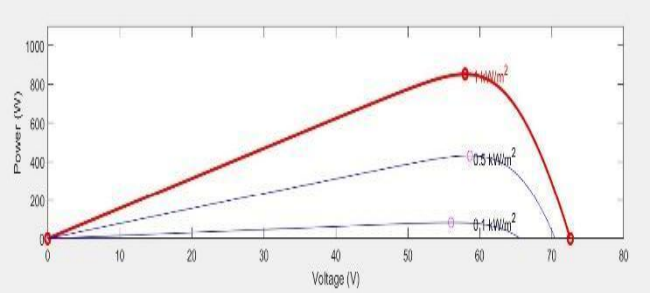

Fig. 7: V-P characteristics curves of the PV array at a specified irradiance

2.2.1 Collecting Data

A thorough simulation using MATLAB/Simulink was undertaken to evaluate the performance of the custom-defined PV array. The objective was to assess how the PV array responds across different levels of solar irradiance (G) and temperature (T), specifically examining its maximum voltage (Vmax) and maximum power (Pmax) outputs. The insights gained from these simulations are essential for gaining a deeper understanding of the efficiency and operational behavior of the PV array [21-23].

1) Simulation Parameters

- *Solar Irradiance (G):* Represents the strength of sunlight reaching the PV array, typically quantified in watts per square meter (W/m²).
- *Temperature (T):* Indicates the surrounding environmental temperature near the PV array, measured in degrees Celsius (°C).

1) Simulation Parameters

- *Diverse Conditions Covered:* The PV array model underwent simulation across a wide spectrum of solar irradiances and temperatures to encompass various environmental scenarios.
- *Utilization of Simulink:* MATLAB/Simulink was employed for conducting simulations, utilizing the detailed PV array model available within the software toolbox.
- *Data Collection:* A total of 104 data points were generated from these simulations, with each point corresponding to specific combinations of solar irradiance (G) and temperature (T). For each data point, the maximum voltage (Vmax) and maximum power (Pmax) values were recorded.

The outcomes from the simulations, encompassing Vmax and Pmax values across different conditions, offer significant insights into how the PV array performs under diverse environmental scenarios [24-26].

The data gathered through MATLAB/Simulink simulations provide a comprehensive perspective on how the PV array functions across various levels of irradiance and temperature. This information is essential for refining and maximizing the efficiency of PV systems in practical settings. By comprehending how environmental factors influence PV output, it becomes possible to make more accurate projections and improvements for renewable energy applications [27].

2.3 DC-DC Ultra Lift Luo Converter Model

The DC-DC Ultra Lift Luo converter represents a sophisticated power electronics component engineered to effectively convert and control voltage levels. It is specifically tailored for applications in photovoltaic (PV) systems, where there is a requirement to elevate the typically low and unregulated output voltage to a level that is suitable for practical use [28].

2.4 Converter Design and Operation

Voltage Lift Technique:

Arithmetic Progression: In basic voltage boosting designs, the output voltage incrementally increases through sequential steps, adhering to a systematic arithmetic pattern. This method ensures a gradual and predictable rise in voltage levels, typically in straightforward voltage conversion and regulation mechanisms.

Geometric Progression: The Ultra Lift Luo converter enhances voltage amplification by utilizing geometric progression. This method results in greater and more efficient increases in output voltage, making the process significantly more effective.

Components and Circuit Design:

The converter employs inductors, capacitors, diodes, and switches arranged strategically to achieve precise voltage alteration according to operational needs. This configuration ensures efficient transformation of electrical energy, maintaining stability and reliability throughout the conversion process, crucial for achieving the intended voltage output reliably and effectively.

The converter's function is based on switching processes that regulate how energy is stored and released in its inductors and capacitors. This controlled energy management leads to a gradual increase in output voltage, which follows a systematic and incremental pattern, akin to an arithmetic progression [29-31].

2.5 Advantages Over Traditional Converters

Higher Voltage Gain

Traditional converters such as Boost, Cuk, and SEPIC are often constrained by their limited ability to increase voltage. In contrast, the Ultra Lift Luo converter stands out for its capability to achieve significantly higher voltage spans, leveraging a geometric progression mechanism that enhances its efficiency and performance in voltage transformation applications [32].

Reduced Harmonics:

Excessive harmonics are problematic as they can interfere with operations and decrease power system efficiency. The Ultra Lift Luo converter effectively mitigates harmonics, resulting in a cleaner and more efficient power output that enhances overall system performance.

Improved Power Factor:

Conventional converters often struggle with undesirable high-power factors, which can result in inefficiencies within the system. In contrast, the Ultra Luo converter is specifically engineered to optimize and maintain a more favorable power factor. This design enhancement ensures that the converter operates more efficiently, minimizing energy losses and improving the overall performance and reliability of the power system.

Higher Efficiency:

The converter enhances efficiency through effective reduction of current ripples, resulting in decreased energy losses and improved overall system performance. By ensuring smoother and more stable current flow, the converter minimizes heat generation and switching losses, optimizing energy usage. This enhanced efficiency not only conserves energy but also enhances the reliability and longevity of connected equipment. Reduced current ripples also contribute to maintaining high power quality, ensuring consistent and reliable operation of electrical systems. Overall, these advancements underscore the converter's ability to operate more efficiently while meeting stringent performance standards and enhancing system reliability.

Higher Voltage Span:

This converter's capability to achieve a broader voltage range makes it well-suited for applications needing significant voltage increases, such as linking photovoltaic systems to external loads.

2.6 Practical Application in PV Systems

Unregulated PV Output:

PV systems typically produce an unregulated output voltage that can vary with changes in solar irradiance and temperature. This unregulated output is often insufficient for directly powering loads or integrating with the grid.

Voltage Regulation:

The Ultra Lift Luo converter plays a vital role in elevating the voltage output of PV systems to a stable, regulated level, making it adaptable for a wide range of applications. This controlled voltage enhancement is essential to ensure the consistency and reliability of power supplied by the PV system, meeting the requirements of different electronic devices and systems. By maintaining a steady output, the converter enables efficient utilization of solar-generated electricity, enhancing overall system performance and reliability [33].

Connection to External Loads:

Utilizing the Ultra Lift Luo converter optimizes the PV system's ability to deliver consistent and reliable power to external loads. This converter guarantees that the voltage output meets specified standards, thereby improving the overall dependability and operational effectiveness of the PV system [34].

The Ultra Lift Luo converter is designed with the following key components:

1. *Switch*

Insulated Gate Bipolar Transistor (IGBT) functions as a semiconductor switch crucial for regulating the converter's duty cycle and operational efficiency.

2. *Diodes*

Standard diodes (D1, D2) are essential components within the circuit, facilitating current flow in one direction while blocking reverse current to maintain proper operation and prevent undesired electrical feedback.

3. *Energy Storage Components:*

Inductors (L1) are utilized to store energy in the form of a magnetic field, facilitating consistent current flow and enhancing the stability of the electrical system. This ensures reliable operation by minimizing fluctuations and maintaining a steady flow of power through the circuit.

Capacitors (C1, C2) also store energy but primarily smooth out voltage fluctuations, ensuring a consistent power supply. Both capacitors have identical values (C2 = C1), contributing equally to the stability and efficiency of the circuit's operation.

The converter employs the ultra-lift technique to consistently elevate the output voltage above the PV array's input voltage. This method incrementally increases the voltage in a geometric progression, ensuring that the output remains positively offset from the input. This design feature guarantees efficient power transformation, essential for maximizing the converter's performance in various applications. It ensures reliable operation by maintaining a stable and suitable output voltage, thereby optimizing the overall efficiency and functionality of the system [35].

The operational dynamics and behavior of the Ultra Lift Luo converter are defined by the set of equations below, which outline its functionality and how it responds to input parameters:

Transfer Gain (K) represents the ratio of the output voltage (Vo) to the input voltage (Vin), elucidating how the converter amplifies the voltage from the input to the output:

$$V_{in} = V_o / K \tag{2}$$

The connection between the input voltage (Vin), output voltage (Vo), and transfer gain (K) is defined by a mathematical equation that outlines how changes in Vin affect Vo, scaled by the factor K. This equation provides a quantitative understanding of how the converter amplifies the input voltage to produce a desired output voltage, crucial for determining its operational characteristics and efficiency in various applications:

$$K = V_o / V_{in} = 1+D / 1-D \tag{3}$$

The output current (Io) in the circuit can be determined using Ohm's law, which states that the current flowing through a conductor between two points is directly proportional to the voltage across the two points and inversely proportional to the resistance between them:

$$V_o = I_o R \tag{4}$$

The DC-DC Ultra Lift Luo converter is an advanced and efficient device designed to elevate voltages without inverting them. It harnesses components like IGBTs, diodes, inductors, and capacitors to achieve substantial voltage increases while ensuring outputs are free from ripples and disturbances. The operational equations it employs are crucial for engineers to effectively design, optimize, and assess the converter's functionality in diverse applications, especially when paired with PV systems. These equations provide insights into how the converter manages voltage transformation, ensuring reliable and efficient power conversion from photovoltaic sources to meet varying electrical demands [36-38].

The DC-DC Ultra Lift Luo converter's operational concept is elucidated by its block diagram, illustrating its key components and how electrical energy moves through the system. This schematic in Fig. 8 offers a comprehensive view of the converter's architecture, showcasing the interplay among components that include IGBTs, diodes, inductors, and capacitors. Understanding these interactions is essential for grasping how the converter achieves efficient voltage elevation without inversion, which is pivotal for its application in diverse electronic and energy systems [39].

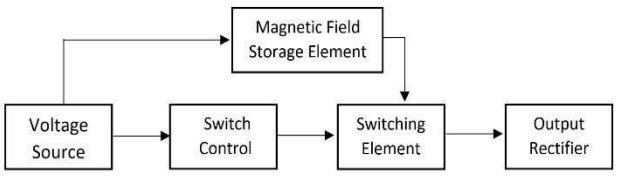

Fig. 8: The Designed Block Diagram of a DC-DC Ultra Lift Luo Converter

The block diagram components and descriptions:
PV Array (Input Voltage Source):

The PV array produces a low and unregulated DC voltage as it converts solar energy into electrical power, which serves as the initial DC input voltage for the converter.

Switch Control:

The component referred to as the Insulated Gate Bipolar Transistor (IGBT) integrates control circuitry responsible for managing the switching function. Through switch control, it modulates the IGBT's duty cycle, thereby regulating energy transfer and directing the switching element to control the voltage conversion process effectively.

The inductor (L1) plays a critical role in the circuit dynamics by harnessing and storing energy within its magnetic field when the switch is turned on.

When the switch deactivates, the inductor releases this stored energy, which helps in stabilizing the current flow and enabling efficient voltage amplification. This cycle of energy storage and release ensures smooth operation of the circuit, minimizing fluctuations and optimizing performance. By managing the flow of electrical energy, the inductor contributes significantly to maintaining stability and enhancing the overall efficiency of the circuit, supporting its function in various electronic applications [40].

Capacitors (Energy Storage):

Two capacitors, C1 and C2, of equal value, function to store and filter energy within the circuit. They work together to ensure a steady output voltage, smoothing fluctuations and minimizing ripple effects, thereby contributing to a consistent and stable electrical output [41-42].

Diodes:

Diodes D1 and D2 serve the purpose of facilitating current flow in a single direction while preventing reverse flow, ensuring efficient energy transfer and supporting voltage elevation by maintaining a unidirectional current path.

2.7 Output Rectifier and Filter

The setup includes capacitors and supplementary diodes designed to guarantee that the output voltage remains stable, devoid of noticeable fluctuations, thereby supplying a consistent high DC voltage to the load.

From equation 3, we computed the output voltage of the DC source, applying Vpv = 10V to the input of the DC-DC Ultra Lift Luo converter. Initiating our block diagram test with a 50% duty cycle, we observed an output voltage of Vo = 32.87V. This

result aligns with the findings illustrated in the simulation design depicted in Fig. 4 [43]. It confirms the converter's ability to efficiently increase the voltage from its initial input, demonstrating its practical functionality in real-world scenarios. The successful outcome underscores the converter's capacity to deliver stable and amplified DC voltage outputs, validating its suitability for applications requiring robust voltage elevation with minimal ripple and high efficiency, as illustrated through comprehensive testing and analysis.

With the DC source providing an input voltage (Vpv = 10V) and applying the designated duty cycle to the DC-DC Ultra Lift Luo converter, we utilize this data to compute the anticipated output voltage (Vo = 32.87V). This calculation hinges on the converter's operational parameters and the relationship between input voltage, duty cycle, and resulting output voltage, as outlined in the converter's specifications and operational principles.

The transfer gain (K) and the equations previously outlined offer insights into how the input voltage relates to the output voltage, elucidating the conversion mechanism. By leveraging these equations, one can comprehend the transformation process from the input to the output voltage within the operational framework of the system.

$$K = V_o / V_{in} = 1+D / 1-D$$
$$K = V_o / V_{in} = 32.87 / 10 = 3.287$$
$$K = 3.287.$$

Now, set up the equation:

$$K = 1+D / 1-D$$

Cross-multiply to solve for D:

$$3.287 \times(1-D) = 1+D$$
$$3.287 -3.287D = 1+D$$
$$3.287 -1 = 3.287D+D$$
$$2.287 = 4.287D$$
$$D = 2.287 / 4.287$$
$$D \approx 0.533.$$

Verify the Gain (K)

Now substitute D = 0.533 back into the gain formula to verify:

$$K = 1+0.533 / 1-0.533$$
$$K = 1.533 / 0.467$$
$$K \approx 3.287$$

The calculated gain K matches our initial calculation, confirming that K ≈ 3.287.

This computation validates the recorded output voltage of 32.87V when supplied with a 10V input and operated at a 50% duty cycle, affirming the accuracy of the simulation's outcomes.

Fig. 9 depicts the experimental setup and simulation outcomes using a block diagram. The results confirm that by employing a 50% duty cycle, the converter effectively increases the input voltage of 10V from the DC source to 32.87V as demonstrated in the Ultra Lift Luo converter's output [45].

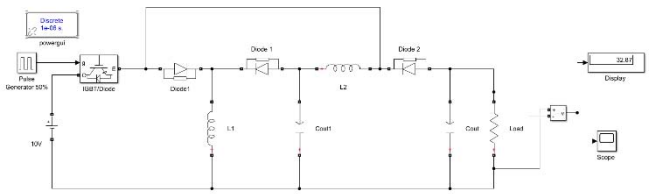

Fig. 9: MATLAB\Simulink of 50% Duty Pulse Generator

The analysis and evaluation using calculations and block diagrams are consistent with the simulation outcomes, confirming the efficacy of the Ultra Lift Luo converter in elevating the voltage from a DC source. This converter efficiently enhances the input voltage, delivering a stable and elevated output voltage suitable for a wide range of applications [46].

The Ultra Lift Luo converter stands out for its efficiency in elevating voltage levels. Fig. 10 illustrates how its output voltage rises swiftly and consistently, demonstrating superior performance compared to conventional converters like Cuk or Boost, which frequently experience overshooting and extended stabilization phases. Both theoretical calculations and simulations confirm the converter's robustness, highlighting its suitability for integrating photovoltaic systems with external loads that demand stable, regulated higher voltages [47-49]. This capability ensures reliable power supply adaptation, crucial for

applications requiring consistent energy delivery without fluctuations, thus enhancing the overall reliability and efficiency of renewable energy systems in practical use scenarios.

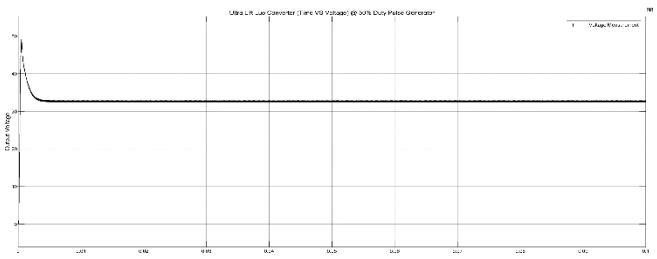

Fig. 10: Ultra Lift Luo Converter Time VS Voltage @ 50% Duty Pulse Generator

III. ARTIFICIAL NEURAL NETWORK (ANN)

Artificial Intelligence (AI) controllers are becoming more prevalent in enhancing the effectiveness and efficiency of photovoltaic (PV) systems. One effective method involves integrating Artificial Neural Networks (ANNs) to optimize the Maximum Power Point (MPP) tracking of PV arrays. This AI-driven approach helps improve overall system performance by dynamically adjusting to changing environmental conditions and maximizing energy output from solar panels [50].

The artificial neural network (ANN) utilized in this proposed design leverages the Levenberg-Marquardt algorithm, renowned for its efficacy and precision in resolving intricate nonlinear least-squares problems. The ANN configuration and application within the PV system are delineated below, elucidating its operational framework and how it optimizes system performance:

3.1 ANN Structure and Training

3.1.1 Input Variables

Solar Irradiance (G): Denotes the measure of solar energy received per unit area at a given location and time, influencing the photovoltaic (PV) array's electricity generation capacity.

Temperature (T): Signifies the environmental heat surrounding the photovoltaic (PV) array, impacting its operational efficiency and output performance.

3.1.2 Network Architecture

The Artificial Neural Network (ANN) is structured with three fundamental layers: an initial input layer that receives data, a middle-hidden layer where computations and transformations occur, and a final output layer that yields the network's results.

Input Layer: At the outset of the network, this foundational layer accepts and processes incoming data elements G and T, representing solar irradiance and ambient temperature, respectively.

Hidden Layers: The hidden layers in the neural network consist of a carefully crafted arrangement of 10 neurons, designed to capture and encapsulate the intricate and nonlinear relationships between input and output data. This configuration is tailored to effectively model the complexity inherent in the system, ensuring robustness in pattern recognition and prediction tasks. While the number of hidden layers can vary, the choice of 10 neurons in each layer for this specific setup underscores the aim to achieve optimal performance in handling the diverse and dynamic nature of the input variables. These hidden layers act as intermediaries, transforming raw data into meaningful representations that facilitate accurate decision-making and system optimization in various applications, including those demanding nuanced processing of data like photovoltaic system management.

Output Layer: The final layer of the neural network functions as the ultimate stage where predictions for both maximum power (Pmax) and maximum voltage (Vmax) are computed. It consolidates and interprets the complex computations from earlier layers, culminating in precise forecasts that are essential for fine-tuning and enhancing the operational efficiency of photovoltaic systems across a spectrum of environmental conditions. This layer plays a critical role in translating the neural network's analytical capabilities into actionable insights, enabling effective management and optimization of photovoltaic system performance [51].

3.1.3 Training Algorithm

The Levenberg-Marquardt Algorithm is chosen for its adeptness in managing intricate data relationships and nonlinearities. Its superiority lies in rapidity and precision, outperforming alternative training methods, thus ideal for applications demanding real-time responsiveness. Training with this algorithm revolves around fine-tuning neural network parameters—such as weights and biases—to minimize the disparity between forecasted and observed Maximum Power Point (MPP) values, ensuring optimal performance in photovoltaic systems [52].

MATLAB/Simulink serves as the platform for simulating and training the Artificial Neural Network (ANN). The neural network undergoes training using a comprehensive dataset encompassing diverse combinations of solar irradiance and temperature inputs. This approach ensures that the network learns effectively and can generalize its predictions to new, previously unseen data points. The integration of MATLAB/Simulink facilitates rigorous testing and optimization of the ANN's performance, making it well-suited for enhancing the efficiency and reliability of photovoltaic systems through accurate Maximum Power Point Tracking (MPPT) capabilities.

3.2 Selecting the Artificial Neural Network (ANN) Structure

In our envisioned setup, we harness the capabilities of an Artificial Neural Network (ANN) to oversee and enhance the Maximum Power Point (MPP) of the photovoltaic (PV) array. This involves utilizing inputs such as solar irradiance (G) and ambient temperature (T) to optimize performance. The ANN's structure and its seamless integration into the PV system are delineated as follows:

Input Layer: The input layer of the artificial neural network (ANN) consists of two neurons specifically designed to handle key variables: Solar Irradiance (G) and Temperature (T). These neurons serve as initial points of entry for integrating environmental data into the ANN, facilitating its capability to interpret and forecast outcomes influenced by fluctuating levels of sunlight intensity and ambient temperature. By processing these crucial environmental factors, the input layer plays a pivotal role in enabling the ANN to make informed decisions regarding the optimal operation of systems such as photovoltaic (PV) arrays. This foundational layer ensures that the network can effectively adjust and adapt its predictions in real-time, enhancing its ability to maximize the efficiency and performance of PV systems under diverse environmental conditions.

Output Layer: The output layer of the neural network comprises two neurons dedicated to key outputs: Voltage (V) and Power (P). These neurons play a critical role in providing the ultimate computed values from the neural network, representing the expected voltage and power outputs based on the operational parameters and environmental conditions of the system. They serve as the final stage in the network's decision-making process, translating complex input data, such as irradiance levels and temperature variations, into actionable voltage and power predictions essential for optimizing the performance of the system in photovoltaic (PV) applications.

Hidden Layer: The hidden layer of a neural network comprises interconnected neurons that use weighted connections to link the input and output layers. The number of neurons in this layer is pivotal, defining the network's ability to model complex nonlinear relationships between input data and desired outputs. More neurons enhance the network's capacity to learn intricate patterns and correlations within data. This layer serves as an intermediary, processing input signals to generate meaningful output predictions based on learned patterns and relationships from the training data. Its role is critical in enabling the network to effectively interpret data and make accurate predictions in various applications.

Network Training: The network is trained using the Levenberg-Marquardt algorithm, renowned for its effectiveness in handling intricate nonlinear challenges with precision. To establish the ideal hidden layer neuron count, a trial-and-error methodology is employed. This involves iteratively adjusting the network's structure until

optimal performance is achieved. The training dataset encompasses diverse G and T values, ensuring the ANN can adeptly handle varying operational scenarios. This methodical approach guarantees the network's robustness and reliability in predicting outcomes, leveraging its ability to discern complex patterns and relationships inherent in the input data [53].

Weighted connections: During training, the weighted connections between the input variables (G and T) and the neurons in the hidden layer are adjusted to improve the accuracy of predicting output values (V and P). This adjustment process is essential for optimizing how the neural network interprets and integrates the input variables, thereby enhancing its ability to forecast voltage and power outputs accurately. This optimization is particularly critical in applications such as solar energy optimization, where precise predictions of voltage and power are vital for maximizing system efficiency and performance under varying environmental conditions. Adjusting these weighted connections ensures that the neural network can effectively capture and utilize the relationships between inputs and outputs, improving overall predictive capability and reliability in practical deployment scenarios.

Prediction of Outputs: The ANN predicts voltage (V) and power (P) by processing input data, optimizing PV system efficiency through continuous adjustment to the Maximum Power Point (MPP). This adjustment dictates the duty cycle for the DC-DC Ultra Lift Luo converter, regulating the Insulated Gate Bipolar Transistor (IGBT) switch. This process ensures maximum renewable energy capture by aligning PV system voltage with load resistances, thereby enhancing overall system performance and energy utilization efficiency.

Influence of Hidden Layers: The efficacy of the ANN hinges on its architecture, particularly the layout of hidden layers and neurons. Experimentation determines the ideal setup for precision and rapidity. In PV systems, these layers play a crucial role in maximizing MPPT efficiency. By meticulously adjusting their configuration through iterative assessment, accuracy, responsiveness, and overall system efficiency are optimized. This method not only bolsters PV system reliability and performance but also promotes the integration of renewable energy solutions in real-world scenarios, marking a significant step toward advancing sustainable energy technologies.

In our simulation framework, the ANN is implemented on MATLAB/Simulink, utilizing the Levenberg-Marquardt algorithm for training and validation. The structure of the ANN, depicted in Fig. 11, includes an input layer for solar irradiance (G) and ambient temperature (T), a hidden layer optimized for neuron count, and an output layer for voltage (V) and power (P). This setup is designed to optimize Maximum Power Point Tracking (MPPT) in PV systems, leveraging neural networks to ensure robust performance across varying environmental conditions. The integration of AI through MATLAB/Simulink's graphical tools facilitates the design, simulation, and analysis of dynamic systems, effectively integrating ANN models with MPPT algorithms and DC-DC converters. Post-training, the ANN provides forecasts of V and P outputs under different irradiance and temperature scenarios, essential for improving the overall efficacy and efficiency of PV systems in renewable energy applications.

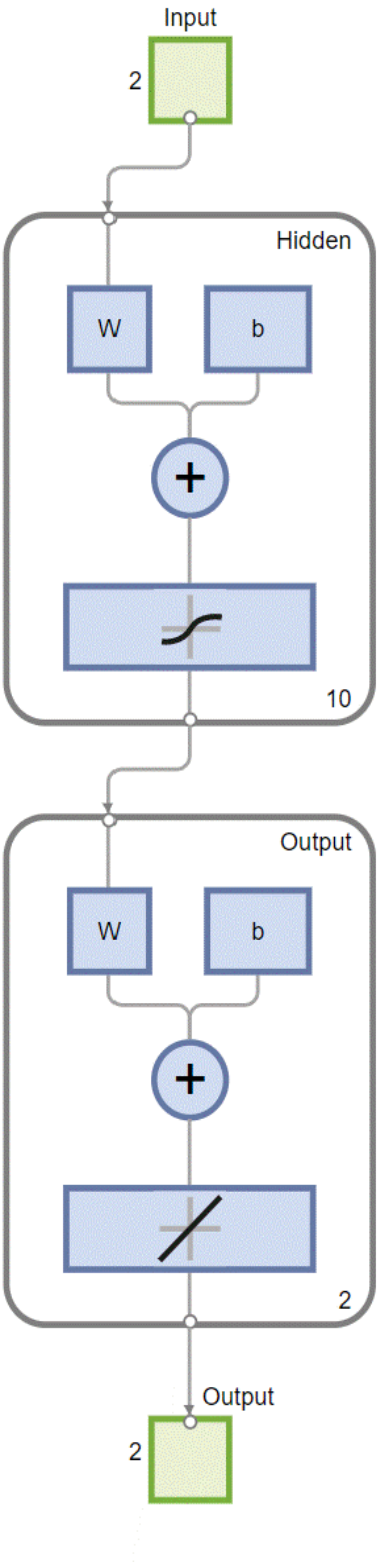

Fig. 11: Proposed ANN structure

Incorporating an Artificial Neural Network (ANN) for Maximum Power Point (MPP) tracking in PV systems marks a notable advancement in system efficiency. Through precise forecasting of the MPP using inputs like irradiance and temperature, the ANN guarantees optimal PV array operation. Training the ANN involves iterative adjustments, supported by the Levenberg-Marquardt algorithm, which effectively manages the PV system's nonlinear traits. Utilizing MATLAB/ Simulink facilitates thorough simulation and testing, verifying dependable performance under diverse conditions. This approach not only enhances accuracy in predicting MPP but also underscores the ANN's capability to streamline renewable energy utilization, making it suitable for practical implementation in various solar energy applications.

To optimize the ANN controller's performance in tracking the MPP of the PV system, various random data sample sets (104, 201, and 1001 points) were rigorously compared to determine the most effective choice for achieving optimal efficiency in MPP tracking.

3.3 Data Sample Sets

104 Random Data Samples:

The ANN controller was trained using an initial dataset that encompassed diverse combinations of irradiance (G) and temperature (T) values, ensuring comprehensive coverage across a wide spectrum of operational scenarios.

201 Random Data Samples:

A larger dataset was curated to introduce greater variability, aiming to enhance the training accuracy and the ANN's ability to generalize across different scenarios.

1001 Random Data Samples:

A substantially increased dataset was curated to encompass a wider range of input variations, enabling the ANN to discern more complex correlations between the input parameters (G and T) and the resultant outputs (V and P). This approach aimed to enrich the model's ability to capture nuanced patterns and optimize its predictive capabilities in solar energy applications.

After completing the training of the ANN controller using each of the three datasets, their

performance was evaluated and compared based on specific criteria:

Accuracy:

The accuracy and reliability of the ANN controller in accurately determining the maximum power point (MPP) by analyzing the provided irradiance and temperature data inputs. This measurement gauges how effectively the controller can predict the optimal operating conditions for maximizing power output from the photovoltaic system under varying environmental factors.

Efficiency:

The effectiveness of the PV system's performance in maximizing energy output using the ANN controller to track the MPP. This capability enhances energy harvesting efficiency, leading to improved overall performance and greater sustainability in harnessing solar energy resources.

Generalization:

The ANN controller's capacity to effectively generalize its predictions to unfamiliar data points, demonstrating its resilience and versatility in varying conditions.

The evaluation of the three datasets (104, 201, and 1001 random samples) resulted in accuracy rates of 91.0380% for 104 samples, 91.1141% for 201 samples, and 92.3221% for 1001 samples. It was found that the ANN controller trained with 1001 random samples outperformed others, benefiting from its ability to capture finer patterns and ensuring superior precision and effectiveness in maximizing the MPP.

Training the ANN with a broad and varied dataset markedly improved the PV system's performance. Among the data sets tested, the ANN trained with 1001 samples proved most effective, ensuring robust and dependable operation under diverse conditions and maximizing efficiency in tracking the MPP.

Upon analysis, the ANN controller trained with 1001 random data samples was integrated into the PV system to ensure consistent MPP tracking, optimize power output, and maintain efficiency across varying environmental conditions. Utilizing MATLAB/Simulink for simulation and training offered a solid foundation to develop and validate the ANN controller, confirming its efficacy for practical implementation in real-world scenarios.

VI. RECURRENT NEURAL NETWORK (RNN)

To improve the PV system's efficiency, an RNN was implemented, leveraging its internal feedback loops to effectively manage time-varying and nonlinear data. This capability is crucial for real-time MPP tracking, enhancing the overall performance and efficiency of the PV array compared to traditional methods.

Feedback Mechanism:

Unlike conventional feedforward neural networks, RNNs utilize feedback loops that enable information retention across sequential steps. This cyclic mechanism empowers the network to preserve context and effectively manage the dynamic and nonlinear characteristics inherent in PV system inputs, distinguishing it as a suitable choice for real-time applications where temporal dependencies are critical.

Training Algorithm:

The training of the RNN involves the application of the Mean Squared Error (MSE) algorithm, a widely adopted method for regression tasks that aims to minimize the squared differences between predicted and actual values. MATLAB/Simulink serves as the platform of choice for implementing and training the RNN, utilizing its robust features to manage intricate simulations and AI training processes effectively.

4.1 RNN Architecture

Input Layer: In the initial stage, the RNN's input layer is configured to intake two specific variables: Solar Irradiance (G) and Temperature (T). These variables are crucial inputs that influence how the RNN processes data, allowing it to adapt and optimize its performance based on varying solar and temperature conditions in real-time applications.

Hidden Layers: The RNN architecture includes 4 hidden layers, with each layer housing 10

neurons. These layers are interconnected to facilitate the network's ability to recognize patterns over time and comprehend intricate correlations within the data, accommodating temporal dynamics and nonlinear interactions effectively.

Output Layer: The output layer represents the culmination of the network's computations, producing a single variable, Voltage (V), which plays a pivotal role in determining the maximum power point (MPP) parameters essential for optimizing photovoltaic system performance. This voltage output is intricately calculated by the RNN through its thorough examination of input data, particularly solar irradiance (G) and temperature (T). Designed with precision, the network operates to forecast and fine-tune this crucial variable, ensuring it aligns optimally with real-time environmental fluctuations. By doing so, the RNN-equipped system achieves superior efficiency in energy harvesting, adeptly adjusting to diverse environmental conditions to maintain robust MPP tracking. This capability not only enhances the overall operational reliability of the PV system but also underscores its adaptability in maximizing renewable energy utilization. Through its sophisticated configuration, the network effectively contributes to the advancement of sustainable energy technologies, leveraging complex algorithms to manage and optimize energy production from solar sources. This integrated approach ensures that the PV system operates at peak efficiency, translating environmental inputs into precise voltage adjustments that enhance overall energy output. In essence, the output layer's function extends beyond mere voltage generation; it represents a critical component in the intelligent management of photovoltaic systems, where accuracy in MPP tracking is paramount for sustainable and effective energy utilization. Thus, the RNN's ability to process and adjust voltage outputs in response to changing environmental variables underscores its role as a cornerstone technology in modern renewable energy applications, paving the way for more efficient and reliable solar power solutions.

Accuracy: The Recurrent Neural Network (RNN) is poised to deliver heightened precision in forecasting the Maximum Power Point (MPP), owing to its capacity to adeptly manage non-linear and time-varying input fluctuations. Photovoltaic (PV) systems manifest non-linear tendencies due to intricate interplays among variables such as solar irradiance (G), temperature (T), and resultant electrical attributes like voltage and current. Leveraging recurrent connections, RNNs excel in capturing these intricate correlations, enabling them to preserve information across sequences of inputs and navigate temporal dependencies effectively. This capability positions RNNs as robust tools for optimizing PV system performance by ensuring accurate MPP tracking under varying environmental conditions, thus enhancing the reliability and efficacy of solar energy utilization.

Response Time: Integrating RNNs into PV systems significantly improves response times compared to conventional ANN controllers due to their inherent recurrent architecture. This design feature allows RNNs to process sequential data and past information, facilitating rapid adaptations to changes in solar irradiance and temperature. By swiftly adjusting parameters to optimize energy capture efficiency, RNNs enhance the overall performance and reliability of PV systems across diverse environmental conditions. This advancement holds substantial promise for advancing renewable energy technologies, ensuring more effective utilization of solar resources and reinforcing the feasibility of sustainable energy solutions in real-world applications.

Efficiency: Efficiency in photovoltaic (PV) systems is significantly bolstered by the integration of Recurrent Neural Networks (RNNs), primarily through their ability to optimize Maximum Power Point (MPP) tracking and swiftly adjust to changes in environmental conditions. This integration results in more precise energy capture and overall system efficiency improvements. By enhancing MPP tracking accuracy, RNNs ensure that PV systems operate at peak performance levels, thus maximizing the economic viability of solar energy while promoting environmental sustainability. This technological advancement represents a pivotal stride in advancing solar PV technology's

capabilities and reliability, underscoring its role in facilitating greater adoption of renewable energy sources worldwide.

4.2 Develop and Train the RNN

Fig. 12 illustrates the development process of the RNN model using MATLAB/Simulink, where critical components such as feedback loops and multiple hidden layers are integrated. The training of the RNN involves utilizing a diverse dataset encompassing various irradiance and temperature inputs, aimed at refining the network's performance through the Mean Squared Error (MSE) algorithm. This approach ensures that the RNN can effectively learn and adapt to the dynamic patterns inherent in solar irradiance and temperature data, enhancing its predictive capabilities. The use of MATLAB/ Simulink provides a robust platform for implementing and fine-tuning the RNN model, enabling thorough testing and validation to optimize its functionality for real-world applications in PV systems.

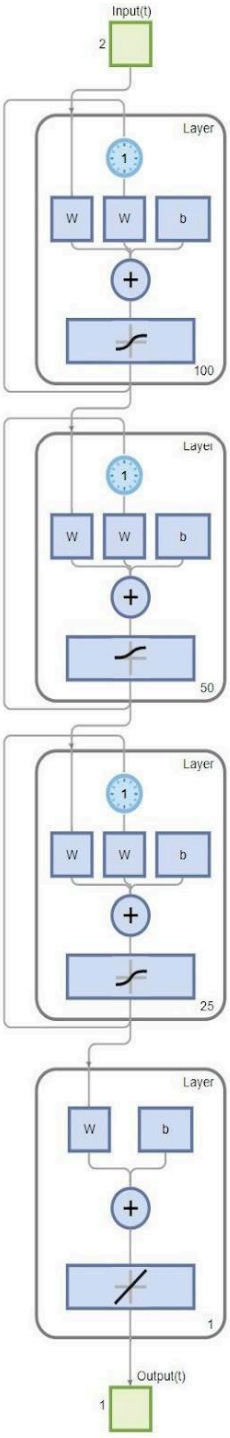

Fig. 12: Proposed RNN structure

The implementation of an RNN to track MPP in PV systems marks a notable stride towards enhanced efficiency. Unlike conventional ANNs, the RNN integrates feedback loops in its internal architecture, enabling better management of the dynamic and nonlinear characteristics of input variables such as solar irradiance and temperature. This capability empowers the RNN to achieve more accurate and responsive adjustments, thereby optimizing energy harvesting and reinforcing its suitability for evolving environmental conditions in solar energy applications.

Harnessing the RNN's functionalities through MSE algorithm training in MATLAB/Simulink enhances the PV system's ability to accurately track MPP. This approach ensures peak performance, effectively maximizing power output and overall system efficiency across varying and unpredictable environmental conditions.

To achieve optimal training and performance of the Recurrent Neural Network (RNN) controller for Maximum Power Point (MPP) tracking in the PV system, we conducted a thorough comparison using various random data sample sizes. The objective was to identify the sample size that best enhances efficiency in MPP tracking. The comparison involved datasets comprising 104, 201, and 1001 random data points to determine the most effective configuration for achieving superior MPP tracking accuracy and efficiency.
Data Sample Sets:

- *104 Random Data Samples:*

This initial dataset consists of fewer samples, facilitating rapid training but potentially restricting the network's capacity to generalize effectively to unseen data points.

- *201 Random Data Samples:*

A moderate-sized dataset strikes a balance, aiming to enhance the network's performance beyond what's achievable with a smaller dataset, while still managing to maintain a reasonable training time.

- *1001 Random Data Samples:*

A substantial dataset covering extensive input conditions enables the RNN to grasp intricate patterns and correlations more comprehensively, potentially resulting in heightened accuracy and efficiency in its operations.

The RNN controller underwent training using the Mean Squared Error (MSE) algorithm within MATLAB/Simulink across all three data sample sets. During training, adjustments were made to the network's parameters to minimize errors in predicting the output voltage (V) based on varying input values of irradiance (G) and temperature (T).

- *Accuracy:*

The accuracy of the RNN controller in forecasting the Maximum Power Point (MPP) under changing irradiance and temperature inputs.

- *Efficiency:*

The effectiveness of the PV system's performance utilizing the RNN controller to optimize the MPP, evaluated through the maximum power generation achieved.

- *Generalization:*

The RNN controller's capability to effectively handle novel data points, demonstrating its resilience and flexibility in adapting to varying conditions.

The evaluation of three different data sample sizes (104, 201, and 1001 random samples) indicated that the RNN controller trained with 1001 random data samples exhibited the highest performance. This larger dataset allowed the RNN to capture more complex patterns, resulting in enhanced accuracy and efficiency in maximizing the system's maximum power point (MPP) tracking.

Training the RNN with a wide-ranging and inclusive dataset markedly improved the PV system's operational effectiveness. Among the various training options explored, the RNN controller trained with 1001 data samples proved optimal, ensuring superior efficiency and consistent performance across diverse environmental scenarios.

Based on these results, the RNN controller trained with 1001 random data samples was integrated into the PV system. This implementation guaranteed consistent MPP tracking, optimal power generation, and efficient operation across

varying environmental conditions. MATLAB/ Simulink facilitated robust simulation and training, validating the RNN controller's efficacy for practical deployment in real-world scenarios.

V. RESULTS AND DISCUSSION FOR ARTIFICAL NEURAL NETWOEK VS RECURRENT NEURAL NETWORK

In Table II, employing a P&O controller achieved an efficiency of 90.8290%. Introducing an ANN controller with 104 samples increased efficiency to 92.7422%, 92.9241% for 201 samples, and 94.8043% for 1001 samples, surpassing the P&O controller's performance. The significant improvement from 104 to 1001 samples highlights the critical role of a larger and diverse dataset in effectively training the ANN controller. Integrating ANN controllers, particularly with extensive sample sizes, markedly enhances PV system efficiency compared to conventional P&O controllers. These findings underscore the efficacy of AI techniques in maximizing power output and enhancing overall system performance across diverse environmental conditions. Implementing an ANN controller for MPP tracking in PV systems notably improves overall efficiency compared to traditional P&O methods. The benefits of larger training datasets are evident in the ANN's enhanced ability to accurately predict and track MPP under varying environmental conditions, ensuring optimal system operation and energy yield.

Table II: Comparison of all used Ann Controllers

No.	Controller Type	Efficiency
1	No controller	80.7254%
2	P&O	90.8290%
3	ANN using 104 Random samples	92.7422%
4	ANN using 201 Random samples	92.9241%
5	ANN using 1001 Random samples	94.8043%

Table III illustrates that employing a P&O controller yielded an efficiency of 90.8290%. Introducing an RNN controller with 104 data samples resulted in an increase to 92.5256%, followed by improvements to 95.8761% and 97.7182% with 201 and 1001 samples, respectively, outperforming the P&O controller. This notable enhancement from 104 to 1001 samples underscores the critical role of a larger and more diverse dataset in effectively training the RNN controller. Integrating RNN controllers, particularly with larger sample sizes, significantly boosts PV system efficiency compared to conventional P&O controllers. These findings underscore the efficacy of AI techniques in maximizing power generation and enhancing overall system performance under varying environmental conditions. Implementing an RNN controller for MPP tracking alongside a DC-DC Ultra Lift Luo converter in PV systems substantially improves overall efficiency compared to traditional P&O methods, particularly with expanded training datasets. These outcomes highlight the RNN's superior capability to precisely predict and maintain MPP under diverse environmental conditions, emphasizing the pivotal importance of dataset size in optimizing performance.

Table III: Comparison of all used Rnn Controllers

No.	Controller Type	Efficiency
1	No controller	80.7254%
2	P&O	90.8290%
3	ANN using 104 Random samples	92.5256%
4	ANN using 201 Random samples	95.8761%
5	ANN using 1001 Random samples	97.7182%

VI. CONCLUSION

In conclusion, our study successfully implemented AI-based ANN and RNN controllers using MATLAB/Simulink to optimize PV system performance. We compared these controllers using varied sample sizes and integrated them with a DC-DC Ultra Lift Luo converter for voltage boosting and impedance matching. Both ANN and RNN controllers predicted maximum output voltage based on nonlinear inputs like irradiance and temperature. The RNN showed superior accuracy and efficiency, especially with a 1001-sample set, highlighting its robust MPP tracking capability. Future research should

explore larger data sets and diverse AI approaches to further enhance PV system efficiency and reliability in real-world applications, advancing renewable energy technology effectively.

REFERENCES

1. K. Mohammad and S. M. Musa, "Optimization of Solar Energy Using Artificial Neural Network Controller," *2022 14th International Conference on Computational Intelligence and Communication Networks (CICN)*, Al-Khobar, Saudi Arabia, 2022, pp. 681-685, doi: 10.1109/CICN56167.2022.10008271.
2. K. A. Mohammad and S. M. Musa, "Optimization of Solar Energy Using Recurrent Neural Network Controller," *2022 14th International Conference on Computational Intelligence and Communication Networks (CICN)*, Al-Khobar, Saudi Arabia, 2022, pp. 1-6, doi: 10.1109/CICN56167.2022.10041248.
3. H. Ibrahim, and N. Anani, "Variations of PV module parameters with irradiance and temperature," Energy Procedia, 2017.
4. K. Razieh, and M. Hamiruce, "Comparison of ANN and P&O MPPT methods for PV applications under changing solar irradiation," IEEE, 2013.
5. A. Mellit, S. Kalogirou, "Artificial Intelligence techniques of sizing photovoltic systems," Renewable Sustainable Energy, 2019.
6. M. Patil and A. Deshpande, "Design and simulation of perturb and observe Maximum Power Point Tracking in MATLAB and Simulink," ICSTM, 2015.
7. K. Jobeda, F. Simon, "Modeling of photovoltaic array in MATLAB Simulink and maximum power point tracking using neural network," Electrical & Electronic Technology Open Access Journal, 2018.
8. K. Ishaque and Z. Salam, " A review of Mazimum Power Point Tracking techniques of PV system for uniform insolation and partial shading condition," Renewable Sustainable Energy Rev, 2013.
9. A. Nasrudin, P. Rahim, "Photovoltaic module modeling using Simulink/Matlab," International Conference on Sustainable Future for Human Security, 2012.
10. M. Samiul, and M. Kamrul, "Design and simulation of maximum poer point traching of photovoltaic system using ANN," ICEEICT, 2016.
11. P. Sahu, and S. Nema, "Physical design and modelling of boost converter for maximum power point traching in solar PV systems," ICEPES, 2016.
12. N. Patcharaprakiti, S. Premrudeepchacharn, "Maximum Power Point Tracking Using Adaptive Fuzzy Logic Control for Grid-Connected Photovoltaic System," IEEE, 2002.
13. S. Azadeh, M. Saad, "Simulation and Hardware Implementation of Incremental Conductance MPPT With Direct Control Method Using Cuk Converter," IEEE, 2011.
14. B. Mark, "Neural Network Toolbox for Use with MATLAB," Book, 2004.
15. G. Kevin, "An introduction to neural networks," Book, 1997.
16. F. Kulsoom, A. Mohammad, "Optimization of Solar Energy Using ANN Techniques," International Conference on Power Energy, 2019.
17. R. Hegazy, "A new MATLAB/Simulink model of triple-junction solar cell and MPPT based on artificial neural networks for photovoltaic energy systems," Ain Shams Engineering Journal, 2015.
18. G. Yu, J Choi, and G. Kim, "A novel two-mode MPPT control algorithm based on comparative study of existing algorithms," Solar Energy, 2004.
19. M. Malik, R Kamara, "A Novel PV based ANN Optimization Converter for off grids Locomotives," ICTAI, 2021.
20. H. Madvar, M Dehghani, and R. Memarzadeh, "Derivation of Optimized Equations for Estimation on Dispersion Coefficient in Natural Stream Using Hybridized ANN With PSO and CSO Algorithms," IEEE, 2020.
21. M. Manimegalai, K. Sebasthiarani, "Efficient Routing in Smart Grid Communication by Secured ABC – ANN Algorithm," IEEE, 2022.
22. H. Elaissaoui, Z. Zerouali, "MPPT Algorithm Based on Fuzzy Logic and Artificial Neural Network (ANN) for a Hybrid Solar/Wide Power Generation System," IEEE, 2020.

23. T. Nguyen, M. Pham, and T. Duong, "A Recent Invasion Wave of Deep Learning in Solar Power Forecasting Techniques Using ANN," IEEE, 2021.
24. O. Savchenko, O. Miroshnyk, "Improving the Efficiency of Solar Power Plants Based on Forecasting the Intensity of Solar Radiation Using Artificial Neural Networks," IEEE, 2021.
25. N. Shyni, M. Linda, "An efficient maximum power point tracking in hybrid solar and wind energy system: A combined AMD-RNN technique," Journal of Intelligent & Fuzzy Systems, 2019.
26. N. Mpho, H. Ali, "Comprehensive Evaluation of Machine Learning MPPT Algorithms," Jornal of Electrical Engineering & Technology, 2020.
27. F. Hassan, E. Ali, "Dynamic global power extraction from partially shaded photovoltaic using deep recurrent neural network and improved PSO techniques," WILEY, 2018.
28. S. Padmanaban, O. Mohammad, "LSTM Recurrent Neural Network Classifier for High Impedance Fault Detection in Solar PV Integrated Power System," IEEE Access, 2021.
29. N. Mpho, H. Ali, "Commensurate Evaluation of Suppoer Vector Machine and Recurrent Neural Network MPPT Algorithm for a PV system under different weather conditions," IEEE, 2020.
30. K. Sudarsan, G. Sreenivasan, "Power Quality Enhancement in Grid Connected Hybrid PV/WT System using Tree Seed Algorithm with RNN," Helix, 2020.
31. V. Kumar, M. Patowary, "Solar Plant Integration to Utility Grid with Improved Power Quality by using RNN-Hebbian-LMS Current Controller," IEEE, 2018.
32. R. Pascanu, T. Mikolov, "On the difficulty of training recurrent neural networks," International Conference on Machine Learning, 2013.
33. L. Sindhura, K. Chaudhary "Artificial Neural Network Implementation for Maximum Power Point Traching of Optimized Solar Power Panel," 2016
34. R. Das, "Application of Recurrent Neural Network using MATLAB SIMULINK in Medicine," Italian Journal of Pure and Applied Mathematics, 2018.
35. Y. Zhang, G. Xiaojiao "MATLAB Simulink Modeling and Simulation of Zhang Neural Network for Online Time-Varying Matrix Inversion," IEEE, 2008.
36. G. Tina, C. Ventura "A State-of-Art-Review on Machine-Learning Based Methods for PV," Applied Science, 2021.
37. A. Toure, D. Tchoffa "Modeling and Control Maximum Power Point Traching of an Autonomous Photovoltaic System Using Atrificial Intelligence," Energy and Power Engineering, 2021.
38. M. Mohamed, C. Ines "A Novel Approach Based Deep RNN Using Hybrid NARX-LSTM Model For Solar Power Forecasting," Aexiv, 2019.
39. M. Nkambule, A. Hasan, A, Ali "Comprehensive Evaluation of Machine Learning MPPT Algorithms for PV Systems Under Different Weather Conditions," JEET 2020.
40. N. Mohan, Department of Electrical and Computer Engineering – University of Minnesota, "First Course on Power Electronics and Drives," 2003.
41. M. Patil, "Modelling and simulation of dc drive using PI and PID controller," International Journal of Innovative Research in Electrical, Electronics, Instrumentation and Control Engineering, vol. 2, pp. 1-15, 2014.
42. N. Ismail, K. Zakaria, N. Nazar, and M. Syaripuddin, "DC motor speed control using a fuzzy logic controller," In AIP Conference Proceedings, vol. 1930, pp. 020026, 2018.
43. M. Ahmad, R. Pankaj, M. Anito, and M. Megha, "Speed Control of a D Motor Using Fuzzy Logic Application," International Journal of Research in Engineering, Technology and Science, vol. 7, pp. 3011, 2018.
44. A. Ahmed, A. Kabir, and M. Shahjahan, IEEE. "Speed control of DC motor with FZ-D controller," 3rd International Conference on Electrical Information and Communication Technology (EICT), pp. 1-6, 2017.
45. K. Passino, S. Yurkovich, and M. Reinfrank, "Fuzzy control," Menlo Park, CA: Addison-Wesley, vol. 42, pp. 15-22, 1998.

46. S. Nasar, "Electric Machines and Transformers," New York: Macmillan, pp.16-18, 1984.
47. H. Beom and H. Cho, "A Sensor-based Obstacle Avoidance Controller for a Mobile Robot Using Fuzzy Logic and Neural Networks," in IEEE International Conference on Intelligent Robots and Systems, pp. 1470-1475, 1992.
48. R. Zulfatman and M. Rahmat, "Application of Self-Tuning Fuzzy PID Controller on Industrial Hydraulic Actuator Using System Identification Approach," Malaysia, pp. 120-132, 2009.
49. R. Arulmozhiyal, and R. Kandiban, "Design of fuzzy PID controller for Brushless DC motor," International Conference on Computer Communication and Informatics, pp. 212-230, 2012.
50. H. Baogang, G. Mann and R. Gosine, "New methodology for analytical and optimal design of fuzzy PID controllers," IEEE Transactions on Fuzzy Systems, vol. 7, pp. 521-539, 1999.
51. H. Li, L. Zhang, K. Cai, and G. Chen, "An improved robust fuzzy-PID controller with optimal fuzzy reasoning," IEEE Transactions on Systems, Man and Cybernetics, vol. 35, pp. 1283-1294, 2005.
52. H. Guoshing, and L. Shuocheng, "PC-based PID speed control in DC motor," International Conference on Audio, Language and Image Processing, pp. 13-22, 2008.
53. MPPT - Search - Search - MATLAB & Simulinkmathworks.com).

This page is intentionally left blank

Structural Equation Model Approach to Understand Intentions to use Online Hospital Services (OHS) in Context of Rural China

Songyu Jiang, Han Wang & Eva Yangyi Ou

Rajamangala University of Technology Rattanakosin

ABSTRACT

This study aims to explore the factors influencing the adoption of Online Hospital Services (OHS) among rural residents in China, utilizing the Technology Acceptance Model (TAM) framework. A Structural Equation Model (SEM) was employed to analyze data collected from 422 participants with Internet hospital experience, selected through random sampling. Data collection involved online questionnaires distributed over 45 days, resulting in effective samples. The survey was divided into six sections, focusing on various aspects of user perceptions and intentions regarding OHS. The results indicate that perceived usefulness (PU) and perceived ease of use (PEOU) positively affect attitudes towards OHS, with trust acting as a crucial mediator between these variables and usage intentions. The study's theoretical contributions include extending TAM by highlighting the central role of trust in digital health adoption, particularly in rural contexts. Practically, the findings suggest that policymakers and technology developers should focus on enhancing trust and user-friendliness to promote OHS adoption, thereby bridging the urban-rural healthcare divide and improving healthcare accessibility.

Keywords: online hospital services; technology acceptance model; perceived usefulness; perceived ease of use; trust.

Classification: DDC Code: 004.9

Language: English

Great Britain Journals Press

LJP Copyright ID: 392954
Print ISSN: 2631-8474
Online ISSN: 2631-8482

London Journal of Engineering Research

Volume 24 | Issue 5 | Compilation 1.0

Structural Equation Model Approach to Understand Intentions to use Online Hospital Services (OHS) in Context of Rural China

Songyu Jiang[α], Han Wang[σ] & Eva Yangyi Ou[ρ]

ABSTRACT

This study aims to explore the factors influencing the adoption of Online Hospital Services (OHS) among rural residents in China, utilizing the Technology Acceptance Model (TAM) framework. A Structural Equation Model (SEM) was employed to analyze data collected from 422 participants with Internet hospital experience, selected through random sampling. Data collection involved online questionnaires distributed over 45 days, resulting in effective samples. The survey was divided into six sections, focusing on various aspects of user perceptions and intentions regarding OHS. The results indicate that perceived usefulness (PU) and perceived ease of use (PEOU) positively affect attitudes towards OHS, with trust acting as a crucial mediator between these variables and usage intentions. The study's theoretical contributions include extending TAM by highlighting the central role of trust in digital health adoption, particularly in rural contexts. Practically, the findings suggest that policymakers and technology developers should focus on enhancing trust and user-friendliness to promote OHS adoption, thereby bridging the urban-rural healthcare divide and improving healthcare accessibility.

Keywords: online hospital services; technology acceptance model; perceived usefulness; perceived ease of use; trust.

Author α: Rattanakosin International College of Creative Entrepreneurship, Rajamangala University of Technology Rattanakosin, 73101. Thailand.
σ: Faculty of Teacher Training, Xishuangbanna Vocational and Technical College, Jinghong, 666100, China.
ρ: Rattanakosin International College of Creative Entrepreneurship, Rajamangala University of Technology Rattanakosin, 73101. Thailand.

I. INTRODUCTION

Online Hospital Services (OHS) leverage internet and information communication technologies to offer comprehensive medical services such as online consultations, remote diagnostics, electronic prescriptions, and health monitoring (Seale et al., 2023). OHS solves the problem of shortage of medical resources in rural areas by allowing residents to obtain diagnostic advice from urban hospitals and experts, thereby improving the accessibility and quality of medical services. OHS also extend high-quality medical resources to remote and underserved areas, promote equality in medical services, and narrow the urban-rural gap (H. Zhang et al., 2023). At the same time, OHS improves the efficiency of medical services through online appointments, remote consultations, and electronic health records, reduce patients' waiting time, optimize resource allocation, and promote long-term health monitoring and management, which helps prevent diseases and promote a healthy lifestyle (Guo et al., 2024). OHS represent an innovative medical model that plays a vital role in improving China's rural medical services by improving accessibility, promoting equity, and improving efficiency (Zhao et al., 2024).

China's OHS has developed rapidly. Since 2020, there have been more than 1,100 Internet hospitals in China, and 7,700 hospitals provide online services ("The Development of E-government," 2023). The online appointment rate of hospitals has reached more than 50%, and 3,300 hospitals have made appointments for treatment in different time periods accurate to 30

minutes. More than 90% of tertiary public hospitals have achieved information sharing within the hospital. The telemedicine collaboration network covers more than 24,000 medical institutions in all prefecture-level cities. 30 provinces have established Internet medical service supervision platforms.

China's OHS have changed the traditional medical methods and patterns, especially bringing new opportunities for the development of medical care in rural China (Wu et al., 2022). However, due to the digital divide and the technological inequality of Internet hospital platforms, the development of rural China is relatively lagging behind (Li & Kostka, 2024). Their understanding and use of Internet hospitals are not mature, and they are not clear about the development trend. On the other hand, due to the large number of medical accidents and medical problems, the trust of residents in rural China in Internet hospitals needs to be solved (Chen et al., 2022).

The using of OHS is beneficial to improve the accessibility and quality of medical services for residents in rural areas, reduce the time and cost of diagnosis and treatment, and achieve more comprehensive health monitoring (Jiang et al., 2022). However, due to the influence of social environment including policies, social media, economic conditions and technical means, their intention to use online hospital services (OHS) needs to be further promoted to promote the digital development of rural medical care and narrow the gap between urban and rural medical digitalization (Pham et al., 2023). On the other hand, the promotion of OHS in rural areas of China obviously faces pressure in terms of publicity and concept shaping (Q. Zhang et al., 2023). Many rural residents lack understanding of the concept and advantages of OHS, believe that face-to-face medical services are more reliable, and have low trust in emerging medical services (Li et al., 2022). This concept is particularly deep-rooted in rural areas

At present, the research on OHS has gradually matured and has achieved some results in health services, drug use and platform construction. However, few studies have focused on the intention of rural residents to use Internet hospitals and narrow the urban-rural medical gap by improving their intention. Therefore, this paper aims to explore the factors that affect the intention of rural residents to use OHS. Specifically, (1) discuss the impact of the usefulness and ease of use of OHS on the attitude and intention to use; (2) explore the mediating role of trust and attitude in the model; (3) provide strategies for the development of rural OHS, encourage villagers to use OHS, and narrow the urban-rural medical gap.

After the introduction, the study introduces relevant theories and concepts and constructs hypotheses. The third part discusses the research methods, followed by the research results. Finally, the study discusses the results, reflecting the theoretical significance and practical value, while also paying attention to the limitations of the study and future research directions.

II. LITERATURE REVIEW

The Technology Acceptance Model (TAM) focuses on the perceived usefulness (PU) and perceived ease of use (PEOU) influencing users' acceptance and adoption of technology (Ge et al., 2023). In the era of digital healthcare, TAM effectively explains patient and healthcare professionals' acceptance behaviors towards Online Hospital Services (OHS) (Li et al., 2023). For patients, PU reflects their perception that using OHS enhances health management efficiency and effectiveness, while PEOU indicates their view that OHS is user-friendly and reduces barriers and cognitive load. From the perspective of healthcare providers, PU manifests in whether systems improve diagnostic and treatment efficiency, and PEOU influences their willingness to adopt new technologies (Al-Momani et al., 2024). In the context of healthcare services and technology, PU refers to whether OHS enhances service quality and efficiency, and PEOU concerns the user-friendliness of platform interfaces and ease of operation. These factors directly impact user trust and intention to continue using the platform (Qin et al., 2023). Therefore, the research hypothesis is:

H1: Perceiving the usefulness of online hospital services can positively influence attitudes towards using OHS.

H2: Perceived ease of use of online hospital services will positively affect attitudes towards using OHS.

H3: The attitude towards using OHS will positively affect the intention to use OHS.

Trust is crucial for users of digital healthcare platforms, facilitating their engagement and acceptance. Consumer trust theories emphasize that trust develops from perceptions of reliability, integrity, and benevolence of the platform provider (Chameroy et al., 2024). Perceived ease of use and usefulness refer to how intuitive and beneficial the platform is perceived to be, influencing trust in the platform during consumer decision-making processes (Le et al., 2022). Consumer trust in Online Hospital Services (OHS) mirrors trust in corporate brands, affecting users' willingness to rely on the platform for sensitive healthcare needs (Qin & Jiang, 2024). In the context of healthcare services, patient trust in hospitals and healthcare providers is paramount (Qin & Jiang, 2024). The usability and utility of digital platforms often shape user trust perceptions, influencing their willingness to share personal health information and engage in telemedicine consultations.

Moreover, trust is multifaceted, encompassing dimensions of competence, integrity, and benevolence. In rural China, shaping trust in medical technology among residents necessitates platform initiatives that promote transparency and reliability (Ye et al., 2022). Enhancing consumer trust in digital healthcare platforms can be achieved through initiatives that foster transparency and reliability in medical service delivery. Therefore, the research hypothesis is:

H4: Perceived the usefulness of online hospital services will positively affect trust in OHS.

H5: Perceived ease of use of online hospital services positively impacts trust in OHS.

Trust often serves as a mediating variable in consumer research because it is fundamental to establishing a sense of security and reliability. For platforms, external factors such as transparency, security measures, and the reputation of service providers drive the construction of trust, influencing users' intentions to adopt technology (Trabucchi et al., 2023). In the context of patient acceptance of medical technology, trust plays a critical role, often cultivated through interactions that shape perceptions and behaviors towards online hospital services (OHS) (Giallanza et al., 2024). Similar to consumer behavior on e-commerce platforms, where trust in social media is fostered through information and system quality, trust in OHS is crucially influenced by factors like data security, healthcare provider credibility, and service reliability. The current challenges of trust in internet hospitals primarily manifest in concerns about data privacy and the competence of virtual healthcare delivery, impacting users' willingness to engage with these technologies (Biancone et al., 2023). Therefore, the study proposes:

H6: Trust in OHS mediates the relationship between perceived usefulness and usage intention of online hospital services.

H7: Trust in OHS mediates the relationship between perceived ease of use and intention to use online hospital services.

H8: Trust in OHS mediates the relationship between perceived usefulness and usage attitude of online hospital services.

H9: Trust in OHS mediates the relationship between perceived ease of use and attitude towards online hospital services.

The consumer trust theory focuses on the role of trust in attitudes and usage intentions. Specifically, trust can reduce the perceived risk of users towards the platform and increase their positive attitudes and usage intentions towards the platform (Nguyen & Llosa, 2023). From the perspective of technological use, trust in new platforms enhances users' sense of security and reliability, promoting their positive attitude and intention towards using the platform (Fu et al., 2021). In the field of medical services, trust is crucial for the attitude and intention of users to use the platform. For example, in the fields of online consultation payment and online health management, trust can increase user acceptance

and willingness to continue using the platform (Liu et al., 2023).Therefore, the study proposes:

H10: Trust in OHS can positively affect attitudes towards using OHS.

H11: Trust in OHS will positively affect the intention to use OHS.

Attitude as an intermediary has been validated in the Technology Acceptance Model (TAM), and from the perspective of technology acceptance, attitude indirectly affects users' intention to use by influencing their perceived usefulness and ease of use (Liesa-Orús et al., 2023). Numerous examples indicate that attitude plays a crucial role in the process of technology adoption (Irimia-Diéguez et al., 2023). In the field of education, students' attitudes towards online learning platforms influence their willingness to use them; In the business field, consumer attitudes towards e-commerce platforms influence their purchasing behavior; In the medical field, the attitude of patients towards online medical platforms affects their intention to use them; In the economic field, investors' attitudes towards financial technology influence their willingness to adopt it. Therefore, the study proposes:

H12: Attitude toward using OHS mediates the relationship between trust and intention to use OHS.

H13: Attitude toward using OHS as a mediator to perceive the relationship between the usefulness of online hospital services and usage intention.

H14: Attitude toward using OHS as a mediator to perceive the relationship between ease of use and intention to use online hospital services.

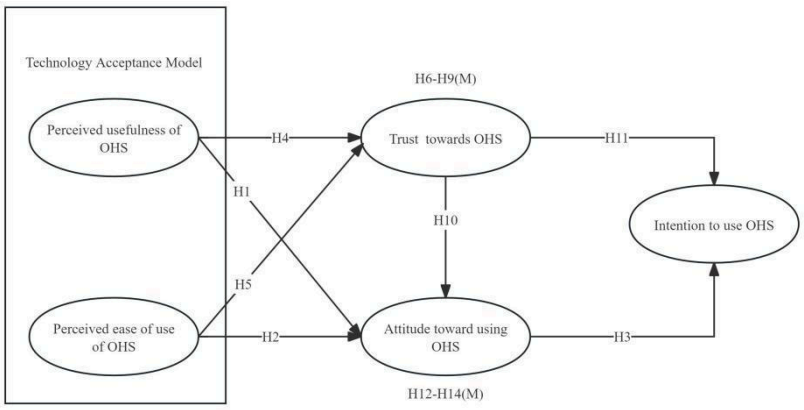

Figure 1: Research model of intention to use online hospital service

III. METHOD

In this study, 422 participants with Internet hospital experience from rural areas in China were investigated by means of online questionnaires. After about 45 days of questionnaire recovery, effective samples were obtained by random sampling.

The survey was divided into six distinct sections, focusing on different aspects of user perceptions and intentions regarding Online Hospital Services (OHS).

The first section is basic information, including gender, age, annual family income (less than 20000, 2-5000, 5-10000, 10-20000, over 200000), education level (without degree, undergraduate degree, undergraduate degree or above, mainly without degree), geographical location (southeast, northwest, central China); Age (18-25, 26-35, 36-45, 46-55, above 55; note that the majority are aged 46 and above, indicating a serious trend of aging in rural areas.)

The second and third sections of the survey investigated perceived usefulness and perceived ease of use, drawing from the foundational studies by Qin et al. (2023) and Venkatesh and Davis (2000). These sections incorporated four items each, designed to explore the constructs across multiple dimensions. This approach aimed to reflect the complexity and multi-faceted nature of

user perceptions towards OHS, capturing elements such as utility, accessibility, user-friendliness, and interface clarity. The fourth section addressed Trust, utilizing scales from Yang et al. (2022) and Fu et al. (2021). It comprised eight items that provided a multidimensional exploration of Trust within the OHS context. This section highlighted specific attributes such as confidentiality, reliability, competence of healthcare providers, and security of medical information, which are crucial for establishing trust in online healthcare platforms. Section five and six explored the Attitude towards and Intention to use OHS, respectively. The items for these sections were inspired by Venkatesh and Davis (2000), structured to assess various dimensions of user attitudes and intentions through a detailed itemized approach. The Attitude section included three items across various dimensions such as satisfaction, perceived benefits, and overall sentiment towards using OHS. Similarly, the Intention section also featured three items, designed to assess the likelihood of continued use, recommendation to others, and trust in the service's efficacy.

All items were structured using a 5-point Likert scale to ensure nuanced data capture. The questionnaire's validity and reliability were confirmed through an Item-Objective Congruence (IOC) process to ensure the professionalism and relevance of the content. Upon data collection, descriptive statistics and basic reliability and validity tests were conducted using statistical software to prepare the data for further analysis. Structural Equation Modeling (SEM) was subsequently employed to perform confirmatory factor analysis and path analysis, which included both direct and indirect effects, providing a robust examination of the hypothesized relationships within the model.

Variables	Items
Perceived Ease of Use	PEU1. I find online hospital services easy to use. PEU2. Learning to operate online hospital services is easy for me. PEU3. I can effectively complete my tasks using online hospital services. PEU4. I believe that interacting with online hospital services is clear and understandable.
Perceived Usefulness	PU1. Using online hospital services enhances my medical management. PU2. Online hospital services improve the results of my medical care. PU3. I find online hospital services to be useful in managing my health. PU4.The information provided by online hospital services is precise and valuable.
Attitude	ATT1. I have a positive attitude towards using online hospital services. ATT2. Using online hospital services is a wise choice for me. ATT3. I feel comfortable using online hospital services.
Intention	INT1. I intend to continue using online hospital services in the future. INT2. I will recommend online hospital services to others. INT3. The probability that I would use online hospital services is high.
Trust towards OHS	TRU1. I believe that the online hospital service provides reliable health information. TRU2. I trust the online hospital service to keep my personal health information secure.

	TRU3. I feel confident in the competency of healthcare professionals available through the online hospital service. TRU4. I am comfortable using the online hospital service for discussing sensitive health issues. TRU5. I trust the online hospital service to offer advice that is in my best interest. TRU6. The privacy policies of the online hospital service are trustworthy. TRU7. I would rely on the online hospital service for urgent health-related advice. TRU8. I believe the online hospital service is consistent in the quality of care it provides.

VI. RESULTS

Table 2 presents the basic demographic information of the sample using online hospital services (OHS) in rural China. 422 balanced rural respondents from all over China, including South China and Central China (21.3%, n=90), East China (20.6%, n=87), West China (18.5%, n=78) and North China (18.2%, n=77). Among them, women accounted for a slightly higher proportion of 53.6% (n=226) and men 46.4% (n=196). The proportion of elderly people in rural areas is very high, with 34.6% (n=146) over 55 years old, and fewer young people staying in the village, with 11.6% (n=49) aged 18-25. Due to the poor education level in rural areas, 64.5% of the population have no degree, only 18.7% (n=79) have a bachelor's degree and 16.8% (n=71) have a degree above the bachelor's level. This also results in their generally low annual family income and a large gap between the rich and the poor, with 20.6% (n=87) earning less than 20,000 yuan. The 20,000-50,000 class has the highest proportion (22.0%, n=93), while the 100,000-200,000 class and the class above 200,000 have the lowest proportions (18.2%, n=77).

Table 2: Essential Information

		Frequency	Percent
Gender	Male	196	46.4
	Female	226	53.6
Age	18-25	49	11.6
	26-35	36	8.5
	36-45	39	9.2
	46- 55	152	36.0
	Greater than 55	146	34.6
Education level	No degree	272	64.5
	Undergraduate degree	79	18.7
	Undergraduate or above	71	16.8
Annual household income	Less than 2w	87	20.6
	2-5w	93	22.0
	5-10w	88	20.9
	10-20w	77	18.2
	Above 200000	77	18.2
Geographical position	Eastern China	87	20.6

	South of China	90	21.3
	Western China	78	18.5
	Northern China	77	18.2
	Central China	90	21.3

Table 3 provides the descriptive statistics of the study variables. The respondents' perceptions of ease of use were generally positive. The mean scores for the PEU items ranged from 3.59 to 3.65, with a standard deviation (SD) close to 1. The skewness values were all negative, ranging from -0.865 to -0.753, with the data distribution slightly skewed to the left, while the kurtosis value was close to zero, indicating a relatively normal distribution. Meanwhile, the perceptions of perceived usefulness were favorable, with mean scores ranging from 3.57 to 3.66, and the SD value was again approximately 1, with the participants' responses being consistent, with skewness values from -0.885 to -0.760, and the kurtosis value close to zero, indicating a slightly leftward skewness, also normally distributed. The attitudes toward using OHS also showed positive mean scores, between 3.59 and 3.66, with similar standard deviation and skewness values, indicating positive attitudes and a normal distribution of the data. The mean scores for intention to use OHS ranged between 3.61 and 3.67, with skewness and kurtosis values showing consistent patterns with the other variables. The mean scores for trust in OHS ranged from 3.57 to 3.69, with slightly smaller skewness values and some kurtosis values indicating a light-tailed distribution.

Table 3: Descriptive Statistics Results

Study variables	Measurement items	Mean	Std. Deviation	Skewness	Kurtosis
Perceived ease of Use of OHS	PEU1	3.630	1.044	-0.834	-0.137
	PEU2	3.650	0.994	-0.753	-0.250
	PEU3	3.590	0.989	-0.865	-0.014
	PEU4	3.640	1.003	-0.828	0.011
Perceived usefulness of OHS	PU1	3.640	0.979	-0.824	-0.033
	PU2	3.570	1.056	-0.760	-0.267
	PU3	3.660	0.969	-0.762	-0.101
	PU4	3.630	0.992	-0.885	0.141
Attitude toward using OHS	ATT1	3.660	1.075	-0.844	-0.089
	ATT2	3.590	0.958	-0.838	0.101
	ATT3	3.610	0.973	-0.892	0.026
Intention to use OHS	INT1	3.610	0.956	-0.815	0.087
	INT2	3.670	0.988	-0.882	0.099
	INT3	3.660	0.990	-0.852	0.032
Trust towards OHS	TRU1	3.620	0.977	-0.804	-0.076
	TRU2	3.600	1.019	-0.772	-0.237
	TRU3	3.690	1.013	-0.759	-0.094
	TRU4	3.630	1.001	-0.768	-0.080
	TRU5	3.650	1.020	-0.712	-0.343
	TRU6	3.600	1.005	-0.606	-0.530
	TRU7	3.570	1.003	-0.828	-0.110
	TRU8	3.610	1.018	-0.752	-0.172

Table 4 presents the reliability statistics for the study variables which showed that the measurement items of various variables in online hospital services (OHS) had good internal

consistency. Specifically, the Cronbach's α coefficients for perceived ease of use and perceived usefulness are 0.834 and 0.840(>0.7), respectively, indicating good internal consistency in the measurement terms of these two variables. The attitude towards using OHS' Cronbach's α=0.787(>0.7), although slightly lower than 0.8, it is still within an acceptable range, indicating that its measurement items have acceptable internal consistency. The intention to use OHS' Cronbach's α=0.800(>0.7), indicating good internal consistency in its measurement terms. The trust in OHS' Cronbach's α=0.900, indicating excellent internal consistency in the measurement of this variable. The measurement items of each variable in the questionnaire have a high level of reliability in evaluating relevant concepts, ensuring data consistency and credibility.

Table 4: Reliability Statistics

Study variables	Number of questions	Cronbach's α
Perceived ease of Use of OHS	4	0.834
Perceived usefulness of OHS	4	0.840
Attitude toward using OHS	3	0.787
Intention to use OHS	3	0.800
Trust towards OHS	8	0.900

Table 5 presents the results of the Kaiser-Meyer-Olkin (KMO) measure of sampling adequacy and Bartlett's test of sphericity, both indicate that the research data on online hospital services (OHS) usage intentions are very suitable for factor analysis. The KMO measure is 0.900, indicating that the sampling is highly suitable for factor analysis. The sample size and correlations among variables are appropriate for conducting a reliable factor analysis. Bartlett's test of sphericity further supports the suitability of the data, with an approximate Chi-Square value of 4131.650, degrees of freedom df =231, and a significance level Sig.=0.000($p < 0.001$) confirms that the correlation matrix is not an identity matrix, indicating significant relationships among variables.Through these tests, researchers can confidently conduct in-depth factor analysis to explore the underlying factors and constructs of online hospital services (OHS) usage intentions.

Table 5: KMO and Bartlett's Test

Kaiser-Meyer-Olkin Measure of Sampling Adequacy.		.900
Bartlett's Test of Sphericity	Approx. Chi-Square	4131.650
	df	231
	Sig.	.000

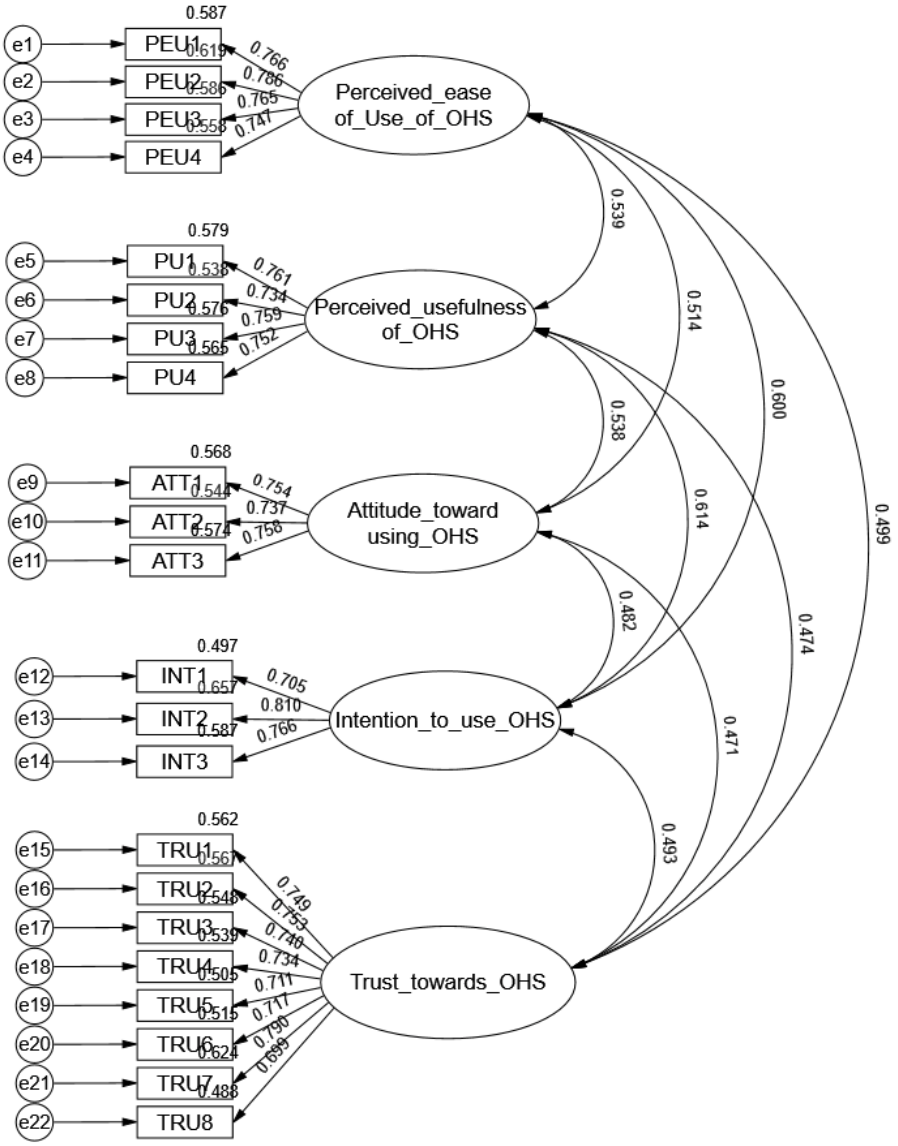

Figure 3: Measurement Model

Table 6 presents the fit metrics for the measurement model that showed good model fit, which verified the validity of the online hospital service (OHS) usage intention model. The chi-square to degrees of freedom ratio $\chi 2/df=1.329(<3)$, indicating a good model fit. The Root Mean Square Error of Approximation (RMSEA)= 0.023(<0.08), suggesting a close fit of the model to the data. The Goodness of Fit Index (GFI) and the Adjusted Goodness of Fit Index (AGFI) are 0.962 and 0.952, respectively, both exceeding their respective benchmarks of 0.9 and 0.85, which further confirms the model's adequacy. Additionally, the Normed Fit Index (NFI), Tucker-Lewis Index (TLI), and Comparative Fit Index (CFI) all surpass the 0.9 standard, with values of 0.959, 0.988, and 0.990, respectively. Table 6 provides a solid foundation for further exploring users' intention to use OHS in rural areas, and supports the application of the model in understanding relevant factors and structures.

Table 6: Measure Model Fit Metrics

Fit index	χ2/df	RMSEA	GFI	AGFI	NFI	TLI	CFI
Reference standards	<3	<0.08	>0.9	>0.85	>0.9	>0.9	>0.9
Result	1.329	0.023	0.962	0.952	0.959	0.988	0.990

Table 7 examines the convergence validity of the measurement model using factor loadings, composite reliability (CR), and average variance extracted (AVE) for each latent variable that evaluated the reliability of the online hospital service (OHS) usage intention model. The factor loadings for all observation indicators exceed the threshold of 0.7, indicating strong individual item reliability. For perceived ease of use (PEU), the factor loadings range from 0.747(>0.7) to 0.786(>0.7), with CR=0.850(>0.7) and AVE=0.587(>0.5), confirming good convergence validity. Similarly, perceived usefulness (PU) exhibits factor loadings between 0.734 and 0.761, CR=0.839, and AVE= 0.565, all of which validate the convergence of this construct. The attitude toward using OHS (ATT) has factor loadings from 0.737 to 0.758, CR= 0.794, AVE = 0.562, demonstrating satisfactory convergence validity. The intention to use OHS (INT) also meets the criteria, with factor loadings from 0.705 to 0.810, CR =0.805, AVE=0.580. Trust towards OHS (TRU) is measured with eight items, showing factor loadings between 0.699 and 0.790, CR=0.905, AVE=0.544, indicating excellent convergence validity. The results indicate that each latent variable has good convergent validity, verifying the internal consistency and reliability of the model, thereby supporting further research on the potential factors and structure of rural users' intention to use OHS.

Table 7: Convergence Validity

Latent variables	Observation indicators	Factor loading	CR	AVE
Perceived ease of Use of OHS	PEU1	0.766	0.850	0.587
	PEU2	0.786		
	PEU3	0.765		
	PEU4	0.747		
Perceived usefulness of OHS	PU1	0.761	0.839	0.565
	PU2	0.734		
	PU3	0.759		
	PU4	0.752		
Attitude toward using OHS	ATT1	0.754	0.794	0.562
	ATT2	0.737		
	ATT3	0.758		
Intention to use OHS	INT1	0.705	0.805	0.580
	INT2	0.810		
	INT3	0.766		
Trust towards OHS	TRU1	0.749	0.905	0.544
	TRU2	0.753		
	TRU3	0.740		
	TRU4	0.734		
	TRU5	0.711		
	TRU6	0.717		
	TRU7	0.790		
	TRU8	0.699		

Table 8 evaluates the discriminant validity of the measurement model in the intention model of online hospital services (OHS) usage using the Fornell-Larcker criterion through discriminant validity testing, where the diagonal elements represent the square root of the Average Variance Extracted (AVE) for each latent variable, and the off-diagonal elements represent the correlations between the constructs.The square roots of perceived ease of use, perceived usefulness, usage attitude, usage intention, and trust were 0.766, 0.752, 0.750, 0.762, and 0.738, respectively, which were higher than the correlation coefficients between the variables, indicating good discriminant validity among the potential variables. These correlation coefficients are 0.539 between perceived ease of use and perceived usefulness, 0.514 between perceived ease of use

and usage attitude, 0.538 between perceived usefulness and usage attitude, 0.614 between perceived usefulness and usage intention, 0.474 between perceived usefulness and trust, 0.482 between usage attitude and usage intention, 0.471 between usage attitude and trust, and 0.493 between usage intention and trust, all of them are significant at the p<0.001. This indicates that the latent variables in the model constructed in this study are significantly different in statistics, verifying the discriminant validity of the model and supporting the reliability and accuracy of the research results on the intention of rural users to use OHS. This further confirms the effectiveness of the model, ensures an understanding of relevant factors and structures, and promotes in-depth exploration of the intention to use online hospital services in rural areas.

Table 8: Discriminant Validity Test

Latent variables	1	2	3	4	5
Perceived ease of Use of OHS	0.766				
Perceived usefulness of OHS	0.539 ***	0.752			
Attitude toward using OHS	0.514 ***	0.538 ***	0.750		
Intention to use OHS	0.600 ***	0.614 ***	0.482 ***	0.762	
Trust towards OHS	0.499 ***	0.474 ***	0.471 ***	0.493 ***	0.738

Note: The diagonal is the square root of the corresponding dimension AVE
****: p<0.001*

Table 9 outlines the model fit metrics for the structural equation model, which are verified the effectiveness of the intention model for rural users to use online hospital services (OHS). The chi-square to degrees of freedom ratio$\chi 2/df=1.783$ (<3), indicating a good fit. The Root Mean Square Error of Approximation RMSEA=0.036 (<0.08), further confirming the model's excellent fit to the data. Additional fit indices include the Goodness of Fit Index GFI=0.950 (>0.9) and the Adjusted Goodness of Fit Index AGFI= 0.937(>0.85), which indicated strong model adequacy. Furthermore, the Normed Fit Index NFI=0.945(>0.9), Tucker-Lewis Index TLI=0.971(>0.9), and Comparative Fit Index CFI =0.975(>0.9). These demonstrate excellent fit across all indices, affirming that the structural equation model robustly represents the underlying data structure.

Table 9: Model Fit Metrics

Fit index	$\chi 2/df$	RMSEA	GFI	AGFI	NFI	TLI	CFI
Reference standards	<3	<0.08	>0.9	>0.85	>0.9	>0.9	>0.9
Result	1.783	0.036	0.950	0.937	0.945	0.971	0.975

Table 10 presents the results of the structural equation model path analysis, verified various hypothetical paths in the intention model for online hospital services (OHS) usage. All the hypothesis are supported, as indicated by the critical ratios C.R.>0.96 and p<0.05, confirming their statistical significance within the 95% confidence interval. PU has a significant positive effect on ATT ($\beta = 0.343$, C.R. = 5.965, $p < 0.001$), supporting H1. Similarly, PEU positively influences ATT ($\beta = 0.278$, C.R. = 4.867, $p < 0.001$), validating H2. The path from ATT to INT is also significant ($\beta = 0.387$, C.R. = 6.909, $p < 0.001$), confirming H3. Furthermore, both PU (β

= 0.295, C.R. = 5.584, p < 0.001) and PEU (β = 0.348, C.R. = 6.543, p < 0.001) significantly influence TRU, supporting H4 and H5. Trust towards OHS (TRU) significantly affects both ATT (β = 0.164, C.R. = 3.189, p = 0.001) and INT (β = 0.325, C.R. = 6.291, p < 0.001), validating H10 and H11. They affirm the robustness of the proposed model in explaining the factors influencing the intention to use online hospital services in rural China, highlighting the critical roles of perceived ease of use, perceived usefulness, and trust in shaping attitudes and intentions.

Table 10: Structural Equation Model Path Test

Hypothesis	Path	Estimate	β	S.E.	C.R.	P	Results
H1	PU→ATT	0.368	0.343	0.062	5.965	***	Supported
H2	PEU→ATT	0.278	0.278	0.057	4.867	***	Supported
H3	ATT→INT	0.325	0.387	0.047	6.909	***	Supported
H4	PU→TRU	0.294	0.295	0.053	5.584	***	Supported
H5	PEU→TRU	0.323	0.348	0.049	6.543	***	Supported
H10	TRU→ATT	0.177	0.164	0.055	3.189	0.001	Supported
H11	TRU→INT	0.295	0.325	0.047	6.291	***	Supported

Note: PEU: Perceived ease of Use of OHS; PU: Perceived usefulness of OHS; ATT: Attitude toward using OHS; INT: Intention to use OHS; TRU: Trust towards OHS.

****: p<0.001*

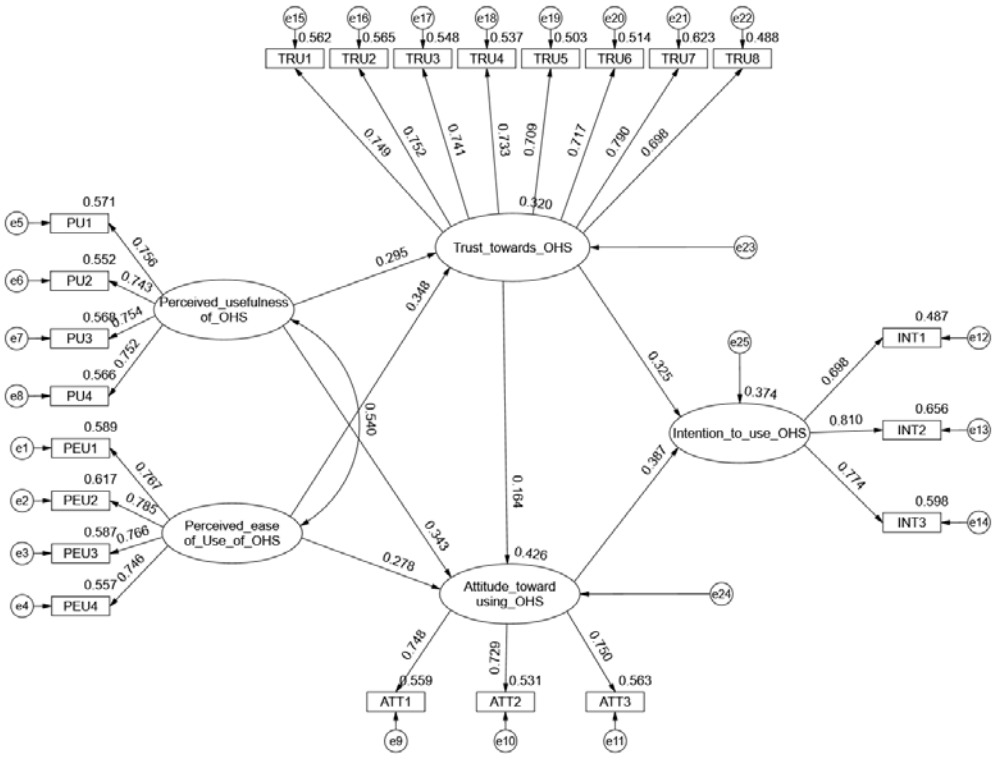

Figure 4: Path Diagram for the Structural Equation Model

Table 11 examines the mediation effects within the structural equation model using a bootstrap test to validate various hypothesized pathways and mediation effects influencing the intention of rural users to use online hospital services (OHS). H6 posits that the effect of PU on INT is mediated by TRU, is supported with an Effect Size = 0.087, SE =0.030, and a 95% CI between 0.037 and 0.155. H7 suggests PEU's influence on INT is mediated by TRU, showing an Effect Size = 0.095,

SE= 0.028, and a 95% CI between 0.053 and 0.166. H8 and H9 test the mediation of TRU on the relationship between PU and ATT, and PEU and ATT. Both paths are supported, with H8 showing an Effect Size =0.052, SE = 0.025, and a 95% CI of 0.005 to 0.110, while H9 has an Effect Size=0.057, SE =0.028, and a 95% CI between 0.006 and 0.122.

Further, H12, examining the mediation effect of ATT on the relationship between TRU and INT, is supported with an Effect Size =0.057, SE =0.027, and a 95% CI of 0.006 to 0.112. H13 and H14 propose that ATT mediates the relationships between PU and INT, and PEU and INT, respectively, are also supported. H13 shows an Effect Size=0.120, SE= 0.040, and a 95% CI of 0.059 to 0.216, while H14 has an Effect Size= 0.090, SE= 0.034, and a 95% CI of 0.034 to 0.171. The bias-corrected confidence intervals for all hypotheses do not include zero, confirming that the mediation effects are statistically significant, thus Tsupport all hypothesized pathways and emphasize the crucial role of trust and usage attitude in the process of users accepting OHS, which provides important theoretical basis for improving the user acceptance and promotion of OHS in rural areas, and also provides empirical support for the formulation and implementation of relevant policies.

Table 11: Mediation Effect Bootstrap Test

Hypothesis	Mediation path	Effect size	SE	Bias-Corrected 95%CI		Results
H6	PU→TRU→INT	0.087	0.030	0.037	0.155	Supported
H7	PEU→TRU→INT	0.095	0.028	0.053	0.166	Supported
H8	PU→TRU→ATT	0.052	0.025	0.005	0.110	Supported
H9	PEU→TRU→ATT	0.057	0.028	0.006	0.122	Supported
H12	TRU→ATT→INT	0.057	0.027	0.006	0.112	Supported
H13	PU→ATT→INT	0.120	0.040	0.059	0.216	Supported
H14	PEU→ATT→INT	0.090	0.034	0.034	0.171	Supported

Note: PEU: Perceived ease of Use of OHS; PU: Perceived usefulness of OHS; ATT: Attitude toward using OHS; INT: Intention to use OHS; TRU: Trust towards OHS.

Table 12 details the total effects of various predictor variables on the intention to use Online Hospital Services (OHS), providing a comprehensive overview of the direct and indirect impacts within the structural model. The effect sizes, standard errors (SE), and bias-corrected 95% confidence intervals (CI) are presented for each path. The effect of perceived ease of use (PEU) on intention to use OHS (INT) has an Effect Size=0.204, SE=0.035, and a 95% CI from 0.144 to 0.289, indicating a significant positive impact. The effect of perceived usefulness (PU) on INT is significant, with an Effect Size=0.223, SE =0.039, and a 95% CI between 0.153 and 0.315. Trust towards OHS (TRU) demonstrates the strongest effect on INT, with an Effect Size= 0.352, SE = 0.060, and a 95% CI from 0.235 to 0.479, underscoring the critical role of trust in shaping users' intentions. The attitude toward using OHS (ATT) also significantly influences INT, with an Effect Size=0.325, SE=0.066, and a 95% CI from 0.213 to 0.481. These results collectively highlight the importance of ease of use, usefulness, trust, and positive attitude in fostering the intention to use online hospital services. The significant total effects, with confidence intervals not including zero, confirm the robustness of the structural model in explaining users' behavioral intentions in the context of rural China's online healthcare services.

Table 12: Total Effect

Effect path	Effect size	SE	Bias-Corrected 95%CI	
PEU→INT	0.204	0.035	0.144	0.289
PU→INT	0.223	0.039	0.153	0.315
TRU→INT	0.352	0.06	0.235	0.479
ATT→INT	0.325	0.066	0.213	0.481

Note: PEU: Perceived ease of Use of OHS; PU: Perceived usefulness of OHS; ATT: Attitude toward using OHS; INT: Intention to use OHS; TRU: Trust towards OHS.

V. DISCUSSION AND CONCLUSION

The study uses a Structural Equation Model to examine the factors influencing rural residents' intentions to use Online Hospital Services (OHS) in China. Utilizing the Technology Acceptance Model (TAM), it investigates how perceived usefulness (PU) and perceived ease of use (PEOU) affect attitudes and trust, subsequently shaping usage intentions. The study reveals that PU and PEOU positively influence attitudes toward OHS, with trust serving as a mediating variable. Trust also mediates the relationship between PU, PEOU, and both attitudes and usage intentions. The research highlights the crucial role of enhancing user trust and optimizing platform usability to promote OHS adoption in rural areas, aiming to bridge the urban-rural healthcare divide and improve overall healthcare accessibility and efficiency. The findings emphasize the need for targeted strategies to boost rural residents' understanding and acceptance of OHS, addressing technological inequalities and fostering a more equitable healthcare system.

5.1 Theoretical Implication

The theoretical contributions of this study to the Technology Acceptance Model (TAM) and the broader field of digital healthcare adoption are significant. Firstly, this research extends TAM by empirically validating the role of trust as a critical mediator between perceived usefulness (PU), perceived ease of use (PEOU), and both attitude and intention to use Online Hospital Services (OHS) among rural residents in China. Previous studies have recognized the importance of PU and PEOU in technology adoption, but this study highlights the indispensable role of trust, which has been less explored in rural healthcare contexts.

By demonstrating that trust mediates the effects of PU and PEOU on attitudes and usage intentions, this research underscores the necessity of fostering trust to enhance the acceptance of digital health platforms. This finding aligns with and expands upon existing literature, which suggests that trust is pivotal in reducing perceived risks and increasing user confidence in technology (Roh et al., 2024). Additionally, the study's context-specific insights into rural healthcare bridge a critical gap in the literature, providing actionable strategies to address technological inequalities and promote equitable healthcare access. The empirical support for these relationships offers a robust framework for policymakers and developers to design and implement more user-centric OHS, ultimately contributing to a more inclusive digital health landscape.

5.2 Practical Implication

The practical implications of this study are multifaceted and relevant for various stakeholders in the digital healthcare ecosystem. For healthcare policymakers, the findings emphasize the importance of fostering trust to increase the adoption of Online Hospital Services (OHS) among rural residents. This can be achieved through rigorous regulations ensuring the security and reliability of these services. Policymakers should focus on creating transparent policies and communication strategies that emphasize the safety and benefits of OHS. Educational

campaigns aimed at increasing awareness about the advantages of OHS, such as reduced travel time and access to specialized care, can significantly alter perceptions and increase trust among rural populations. Additionally, integrating community leaders and healthcare professionals in these campaigns can help bridge the trust gap, as these figures often hold significant influence in rural areas.

For technology developers and healthcare providers, the study highlights the need to design user-friendly and intuitively designed platforms that cater to the specific needs of rural users. Given that perceived ease of use directly impacts trust and adoption intentions, developers should prioritize simplicity in interface design and ensure that the platforms are accessible even to those with limited digital literacy. Training programs for healthcare providers on how to effectively use OHS can further enhance the service delivery, ensuring that the technology is used to its full potential. Moreover, incorporating feedback mechanisms where users can report issues or provide suggestions can help in continually improving the service and maintaining user trust. Ensuring high-quality, consistent care and protecting patient data are crucial steps towards building a trustworthy digital healthcare environment. Overall, these actions can lead to a more inclusive and efficient healthcare system that bridges the urban-rural healthcare divide.

5.3 Conclusion

This study provides significant theoretical and practical insights into the adoption of Online Hospital Services (OHS) among rural residents in China by extending the Technology Acceptance Model (TAM). The research confirms that perceived usefulness (PU) and perceived ease of use (PEOU) positively influence attitudes toward OHS, with trust playing a crucial mediating role. This highlights the necessity of enhancing user trust to promote the acceptance of digital health platforms. The findings emphasize the importance of creating user-friendly interfaces and fostering trust through transparent policies and robust security measures. These insights are crucial for policymakers and technology developers aiming to bridge the urban-rural healthcare divide and promote equitable healthcare access.

However, this study has certain limitations that provide avenues for future research. The sample is restricted to rural residents in China, which may limit the generalizability of the findings to other contexts or countries. Future research could expand the demographic scope to include diverse populations and settings. Additionally, while the study highlights trust as a mediating factor, it does not explore other potential mediators or moderators such as cultural factors, socioeconomic status, or prior experiences with digital technology. Further investigation into these aspects could provide a more comprehensive understanding of OHS adoption. Longitudinal studies could also be conducted to assess how attitudes and trust in OHS evolve over time, providing deeper insights into the long-term impacts of digital healthcare interventions.

REFERENCES

1. Al-Momani, A. a. M., Ramayah, T., & Al-Sharafi, M. A. (2024). Exploring the impact of cybersecurity on using electronic health records and their performance among healthcare professionals: A multi-analytical SEM-ANN approach. *Technology in Society*, *77*, 102592. https://doi.org/https://doi.org/10.1016/j.techsoc.2024.102592 .
2. Biancone, P., Secinaro, S., Marseglia, R., & Calandra, D. (2023). E-health for the future. Managerial perspectives using a multiple case study approach. *Technovation*, *120*, 102406. https://doi.org/https://doi.org/10.1016/j.technovation.2021.102406.
3. Chameroy, F., Salgado, S., de Barnier, V., & Chaney, D. (2024). In platform we trust: How interchangeability affects trust decisions in collaborative consumption. *Technological Forecasting and Social Change*, *198*, 122997. https://doi.org/https://doi.org/10.1016/j.techfore.2023.122997.
4. Chen, Q., Xu, D., Fu, H., & Yip, W. (2022). Distance effects and home bias in patient choice on the Internet: Evidence from an online healthcare platform in China. *China Economic Review*, *72*, 101757. https://doi.

org/https://doi.org/10.1016/j.chieco.2022.101757.
5. The Development of E-government. (2023). In *China Internet Development Report 2021: Blue Book for World Internet Conference* (pp. 55-84). Springer Nature Singapore. https://doi.org/10.1007/978-981-19-9311-4_4.
6. Fu, Y., Tang, T., Long, J., Lin, B., Li, J., Quan, G., Yang, H., Zhao, C., Yin, M., & Shi, L. (2021). Factors associated with using the internet for medical information based on the doctor-patient trust model: a cross-sectional study. *BMC Health Services Research*, *21*(1), 1268. https://doi.org/10.1186/s12913-021-07283-6
7. Ge, Y., Qi, H., & Qu, W. (2023). The factors impacting the use of navigation systems: A study based on the technology acceptance model. *Transportation Research Part F: Traffic Psychology and Behaviour*, *93*, 106-117. https://doi.org/https://doi.org/10.1016/j.trf.2023.01.005.
8. Giallanza, A., La Scalia, G., Micale, R., & La Fata, C. M. (2024). Occupational health and safety issues in human-robot collaboration: State of the art and open challenges. *Safety science*, *169*, 106313. https://doi.org/https://doi.org/10.1016/j.ssci.2023.106313.
9. Guo, H., Xie, Y., Jiang, B., & Tang, J. (2024). When outpatient appointment meets online consultation: A joint scheduling optimization framework. *Omega*, *127*, 103101. https://doi.org/https://doi.org/10.1016/j.omega.2024.103101.
10. Irimia-Diéguez, A., Velicia-Martín, F., & Aguayo-Camacho, M. (2023). Predicting Fintech Innovation Adoption: the Mediator Role of Social Norms and Attitudes. *Financial Innovation*, *9*(1), 36. https://doi.org/10.1186/s40854-022-00434-6.
11. Jiang, Y., Sun, P., Chen, Z., Guo, J., Wang, S., Liu, F., & Li, J. (2022). Patients' and healthcare providers' perceptions and experiences of telehealth use and online health information use in chronic disease management for older patients with chronic obstructive pulmonary disease: a qualitative study. *BMC geriatrics*, *22*(1), 9. https://doi.org/10.1186/s12877-021-02702-z.
12. Le, L. T., Ly, P. T. M., Nguyen, N. T., & Tran, L. T. T. (2022). Online reviews as a pacifying decision-making assistant. *Journal of Retailing and Consumer Services*, *64*, 102805. https://doi.org/https://doi.org/10.1016/j.jretconser.2021.102805.
13. Li, H., & Kostka, G. (2024). Navigating the digital age: The gray digital divide and digital inclusion in China. *Media, Culture & Society*, 01634437241229382. https://doi.org/10.1177/01634437241229382.
14. Li, J., Zhao, N., Zhang, H., Yang, H., & Yang, J. (2022). Roles and Challenges for Village Doctors in COVID-19 Pandemic Prevention and Control in Rural Beijing, China: A Qualitative Study. *Frontiers in public health*, *10*. https://www.frontiersin.org/journals/public-health/articles/10.3389/fpubh.2022.888374.
15. Li, W., Gui, J., Luo, X., Yang, J., Zhang, T., & Tang, Q. (2023). Determinants of intention with remote health management service among urban older adults: A Unified Theory of Acceptance and Use of Technology perspective. *Frontiers in public health*, *11*. https://www.frontiersin.org/journals/public-health/articles/10.3389/fpubh.2023.1117518.
16. Liesa-Orús, M., Latorre-Cosculluela, C., Sierra-Sánchez, V., & Vázquez-Toledo, S. (2023). Links between ease of use, perceived usefulness and attitudes towards technology in older people in university: A structural equation modelling approach. *Education and Information Technologies*, *28*(3), 2419-2436. https://doi.org/10.1007/s10639-022-11292-1
17. Liu, J. Y. W., Sorwar, G., Rahman, M. S., & Hoque, M. R. (2023). The role of trust and habit in the adoption of mHealth by older adults in Hong Kong: a healthcare technology service acceptance (HTSA) model. *BMC geriatrics*, *23*(1), 73. https://doi.org/10.1186/s12877-023-03779-4.
18. Nguyen, S., & Llosa, S. (2023). When users decide to bypass collaborative consumption platforms: The interplay of economic benefit, perceived risk, and perceived enjoyment. *Tourism Management*, *96*, 104713. https://doi.org/https://doi.org/10.1016/j.tourman.2022.104713.

19. Pham, T. T., Lingard, H., & Zhang, R. P. (2023). Factors influencing construction workers' intention to transfer occupational health and safety training. *Safety science*, *167*, 106288. https://doi.org/https://doi.org/10.1016/j.ssci.2023.106288.
20. Qin, P., & Jiang, S. (2024). Toward Digital Hospital Services: Developing an Integrated Model to Understand Patient Intentions for Utilizing Online Hospital Service Platforms. *Journal of Electrical Systems*, *20*(6(S)), 880-896. https://doi.org/10.52783/jes.2768
21. Qin, P., Yang, H., & Jiang, S. (2023). Exploring the Users' Intention to Use Online Hospital Service Platform Based on Extend UTAUT. *Migration Letters*, *20*(S11), 813-832. https://doi.org/10.59670/ml.v20iS11.5780
22. Roh, T., Yang, Y. S., Xiao, S., & Park, B. I. (2024). What makes consumers trust and adopt fintech? An empirical investigation in China. *Electronic Commerce Research*, *24*(1), 3-35. https://doi.org/10.1007/s10660-021-09527-3.
23. Seale, D. E., LeRouge, C. M., & Kolotylo-Kulkarni, M. (2023). A Description of Personal Health Information Management Work With a Spotlight on the Practices of Older Adults: Qualitative e-Delphi Study With Professional Organizers. *Journal of medical Internet research*, *25*, e42330.
24. Trabucchi, D., Patrucco, A. S., Buganza, T., & Marzi, G. (2023). Is transparency the new green? How business model transparency influences digital service adoption. *Technovation*, *126*, 102803. https://doi.org/https://doi.org/10.1016/j.technovation.2023.102803.
25. Venkatesh, V., & Davis, F. D. (2000). A theoretical extension of the technology acceptance model: Four longitudinal field studies. *Management science*, *46*(2), 186-204.
26. Wu, H., Ba, N., Ren, S., Xu, L., Chai, J., Irfan, M., Hao, Y., & Lu, Z.-N. (2022). The impact of internet development on the health of Chinese residents: Transmission mechanisms and empirical tests. *Socio-Economic Planning Sciences*, *81*, 101178. https://doi.org/https://doi.org/10.1016/j.seps.2021.101178.
27. Yang, M., Jiang, J., Kiang, M., & Yuan, F. (2022). Re-Examining the Impact of Multidimensional Trust on Patients' Online Medical Consultation Service Continuance Decision. *Information Systems Frontiers*, *24*(3), 983-1007. https://doi.org/10.1007/s10796-021-10117-9.
28. Ye, L., Dai, Y., & Dong, X. (2022). The enabling mechanism of shuren culture in ICT4D: A case study of rural China. *Technology in Society*, *68*, 101842. https://doi.org/https://doi.org/10.1016/j.techsoc.2021.101842.
29. Zhang, H., Zhou, B.-B., Liu, S., Hu, G., Meng, X., Liu, X., Shi, H., Gao, Y., Hou, H., & Li, X. (2023). Enhancing intercity transportation will improve the equitable distribution of high-quality health care in China. *Applied Geography*, *152*, 102892. https://doi.org/https://doi.org/10.1016/j.apgeog.2023.102892.
30. Zhang, Q., Oo, B. L., & Lim, B. T. H. (2023). Unveiling corporate social responsibility awareness and implementation: a study of the Chinese construction firms. *Journal of Environmental Planning and Management*, *66*(9), 1861-1889. https://doi.org/10.1080/09640568.2022.2043258.
31. Zhao, Y., Qiao, Q., Xu, X., & Bian, Y. (2024). Effectiveness of hierarchical medical system and economic growth: based on China's urban vs. rural health perspectives [Original Research]. *Frontiers in public health*, *12*. https://www.frontiersin.org/journals/public-health/articles/10.3389/fpubh.2024.1364584.

Great Britain Journal Press Membership

For Authors, subscribers, Boards and organizations

Great Britain Journals Press membership is an elite community of scholars, researchers, scientists, professsionals and institutions associated with all the major disciplines. Great Britain memberships are for indivi - duals, research institutions, and universities. Authors, subscribers, Editorial Board members, Advisory Board members, and organizations are all part of member network.

Read more and apply for membership here:
https://journalspress.com/journals/membership

Author Membership provide access to scientific innovation, next generation tools, access to conferences/seminars/ symposiums/webinars, networking opportunities, and privileged benefits. Authors may submit research manuscript or paper without being an existing member of GBJP. Once a non-member author submits a research paper he/she becomes a part of "Provisional Author Membership".

Society flourish when two institutions Come together." Organizations, research institutes, and universities can join GBJP Subscription membership or privileged "Fellow Membership" membership facilitating researchers to publish their work with us, become peer reviewers and join us on Advisory Board.

Subscribe to distinguished STM (scientific, technical, and medical) publisher. Subscription membership is available for individuals universities and institutions (print & online). Subscribers can access journals from our libraries, published in different formats like Printed Hardcopy, Interactive PDFs, EPUBs, eBooks, indexable documents and the author managed dynamic live web page articles, LaTeX, PDFs etc.

PRINTED VERSION, INTERACTIVE PDFS, EPUBS, EBOOKS, INDEXABLE DOCUMENTS AND THE AUTHOR MANAGED DYNAMIC LIVE WEB PAGE ARTICLES, LATEX, PDFS, RESTRUCTURED TEXT, TEXTILE, HTML, DOCBOOK, MEDIAWIKI MARKUP, TWIKI MARKUP, OPML, EMACS ORG-MODE & OTHER